Multiple Sclerosis Lesions Identification/Segmentation in Magnetic Resonance Imaging using Ensemble CNN and Uncertainty Classification

Giuseppe Placidi[1*]   Luigi Cinque[2]   Filippo Mignosi[3]   Matteo Polsinelli[1]

[1] A2VI-lab, c/o Department of MeSVA, University of LAquila, Via Vetoio Coppito 2, 67100 - LAquila, ITALY
giuseppe.placidi@univaq.it
[2] Department of Computer Science, Sapienza University of Rome, Via Salaria 113, 00198 - Roma, ITALY
[3] Department of DISIM, University of LAquila, Via Vetoio Coppito, 67100 - LAquila, ITALY

Abstract

To date, several automated strategies for identification/segmentation of Multiple Sclerosis (MS) lesions by Magnetic Resonance Imaging (MRI) have been presented which are either outperformed by human experts or, at least, whose results are well distinguishable from humans. This is due to the ambiguity originated by MRI instabilities, peculiar MS Heterogeneity and MRI unspecific nature with respect to MS. Physicians partially treat the uncertainty generated by ambiguity relying on personal radiological/clinical/anatomical background and experience.

We present an automated framework for MS lesions identification/segmentation based on three pivotal concepts to better emulate human reasoning: the modeling of uncertainty; the proposal of two, separately trained, CNN, one optimized with respect to lesions themselves and the other to the environment surrounding lesions, respectively repeated for axial, coronal and sagittal directions; the ensemble of the CNN output.

The proposed framework is trained, validated and tested on the 2016 MSSEG benchmark public data set from a single imaging modality, FLuid-Attenuated Inversion Recovery (FLAIR). The comparison, performed on the segmented lesions by means of most of the metrics normally used with respect to the ground-truth and the 7 human raters in MSSEG, prove that there is no significant difference between the proposed framework and the other raters. Results are also shown for the uncertainty, though a comparison with the other raters is impossible.

1   Introduction

Multiple Sclerosis (MS) is a degenerative disease affecting white matter (WM) and spinal cord, with very heterogeneous clinical presentation across patients both in severity and symptoms [65]. Also its clinical course is unpredictable and most patients are initially diagnosed as having relapsing-remitting MS characterized by inflammatory attacks interleaved by variable periods of remission and recovery. After the first phase, a second stage follows consisting on unremitting and progressive accumulation of disability. This means that, in the same patient, lesions in different status often coexist at the same time, in different locations and could variate in shape and intensity. Furthermore, often partial volume effect (PVE) occurs when lesions and healthy tissue are present in the same place.

At present there are no definitive cures and therapies are focused on symptoms attenuation and prevention of further damages through the monitoring of signs and drug modulation. The origins of the disease are not well understood but characteristic signs of tissue degeneration are recognizable as white matter lesions and brain atrophy or shrinkage. Most of these signs can be observed by Magnetic Resonance Imaging (MRI) which has become the elective mini-invasive tool for MS monitoring [22]. Focal lesions in the brain and spinal cord are primarily visible in the white matter on structural MRI

---

observable as hyper-intensities on T_2-weighted images (T_2w), proton-density images (PD), or fluid-attenuated inversion recovery images (FLAIR), and as hypo-intensities on T_1-weighted images (T_1w).

Physicians often use FLAIR images for WM lesion detection and other modalities mostly for ascertain lesion status. Complementary information are collected to visualize cortical lesions by means of MPRAGE and MP2RAGE imaging sequences [10, 38, 48].

An examination consists of thousands of images mostly collected pre and post contrast agent administration. MRI is used routinely in clinical practice but it is unspecific for MS and not well correlated to clinical disability progression (physical and cognitive), to neuro-plasticity and to the effects of demyelinization of nerves, a critical effect which is invisible to MRI. Indeed, WM could appear normal though it has reduced myelin: for a MS patient, the "healthy" brain tissue is usually referred as "apparently healthy" [22]. Healthy anatomical structures similar to lesions and close to lesions could contribute to create further ambiguity.

Regarding MRI, there is a huge variability in images due to differences in scanners, magnetic field strength/homogeneity and tuning of parameters [50]. Some effort has been made to standardize MRI as for computed tomography [16] but results are still unsatisfactory due to the huge set of parameters to be controlled.

As a consequence, MRI and MS heterogeneity, coupled to similarity between lesions and healthy tissues and to PVE, often create uncertainty, ambiguities and disagreement between radiologists (inter-raters variability) and doubts in a same radiologist (intra-rater variability) mainly in defining the borders of the lesions but also in defining some regions as being lesions or not. This could make manual segmentation, besides long and boring, also inaccurate, especially when quantitative evaluations are required.

However, expert radiologists fast adapt themselves to implicit contrast variations in MRI and tend to manage part of the uncertainty by relying on unexpressed and implicit anatomical/clinical background, knowledge about symptoms and experience on MS in general. Despite that, residual uncertainty remains due to PVE, to the unspecific role of MRI for MS and to MS intrinsic variability.

Specific automatic frameworks have been recently proposed and reviewed [4, 19, 21, 26, 27, 37, 75] also for evaluating MS temporal progression [25, 52, 59]. However, to date the results are still far from those of human experts, though the efforts trough the increasing of model/architectural complexity. Indeed, often state of the art methods failed when tested on data from different data set [44]. This mainly occurs because automated strategies are not robust to MRI variability, are sufficiently able to model medical knowledge, human operational capacity and flexibility.

Regarding implicit medical knowledge and experience, they mostly remain unexpressed and are not reported on the labelled data sets used to train the automatic strategies.

The same regards the reasoning methodology used by radiologists during 3D data analysis: data are mostly analyzed in 2D axial slices with a continuous view of coronal and sagittal slices to confirm an hypothesis, to give spatial continuity to a lesion or to check the environment in which the hypothetical lesion is located [22, 67].

Indeed, not even the uncertainty affecting expert radiologists when classifying some regions, is indicated into the public datasets used for training: a binary result not ever represent the right evaluation of an expert. If represented, the uncertainty could greatly help an automatic strategy to segment better also undoubted lesions [rifs]. This pushed several scientists to investigate on uncertainty in medical data [5, 47].

Implicit information in automated methods have had no room or, introduced with external supports (dictionary, anatomical atlases, etc.), are probably insufficient as far as the gap with human experts remains.

We aim at filling this gap, both in performance and in reasoning, by proposing a framework which includes: 1) the classification of uncertainty as an intermediate class between the background and lesions; 2) the optimization of two CNN, one for the class lesion and one for the class background to contextualize lesions with respect to the surrounding anatomical structures, for the three spatial directions axial, coronal and sagittal; 3) the definition of an ensemble classifier to merge the information collected by all CNN.

To obtain our goal we: use the publicly available large-scale benchmark MRI database and corresponding ground truth proposed in 2016 MICCAI MS Lesion Segmentation Challenges, MSSEG [1]; define the uncertain regions with the help of the binary classifications of 7 human raters in MSSEG; apply the framework just on FLAIR images. The reasons of these choices are to: compare the proposed framework with competitive automated strategies and human experts; demonstrate that to model the uncertainty reasoning could help in reducing the ambiguity and complexity of the, intrinsically uncertain, problem; demonstrate that a single imaging sequence, FLAIR, is sufficient for MS lesion identifica-

tion/segmentation in WM. It is implicit that, the framework is just applied on WM lesions and not on cortical lesions: data from MPRAGE and MP2RAGE are available in MSSEG.

Relevant contributions of the manuscript are: the usage of uncertainty to emulate uncertain reasoning and to improve lesion identification/segmentation; the contemporary exploitation of lesions and lesions in the context of the surrounding environment; the ensemble of CNN-based automated raters approaching the problem by different points of view; the demonstration that just a single MRI modality, FLAIR, is sufficient to classify/segment MS lesions from WM; the demonstration that an automatic strategy behave and perform like a human expert.

The remaining of the manuscript is structured as follows: Section 2 presents a review of automatic approaches to MS lesions identification/segmentation, in particular those using CNNs; Section 3 describes the proposed framework in the context of the used data set, of the defined three-class consensus used for training, the proposed CNN architecture and the ensemble system; Section 4 details the metrics used for comparison; Section 5 reports and discusses experimental results; Section 6 concludes the paper and presents some constructive hints for future improvements.

2   Related work

Medical image analysis is greatly performed with automated methods, mostly involving deep learning [42]. Automated MS lesion identification/segmentation is still an active field of research and several methods have been provided in the last decade and well reviewed along time [19, 21, 23, 37, 43, 46, 75] and the role of AI-based methods is emerging [2]. Automated strategies can be classified in three main groups: methods using pre-selected features (PSFM), methods using a-priori information (APIM) and methods using deep learning (DLM).

PSFM calculate pre-selected features and learn from previously segmented training images to separate lesions from healthy tissue [78]. Some PSFM use large set of features and select the more discriminant ones through labelled training. One of the first, an atlas based technique employing topological and statistical atlas for WM lesion segmentation, is described in [62]. Another method includes the usage of decision random forests [24]. Similarly, a framework for segmentation of contrast-agent enhanced lesions using conditional random fields is defined in [34]. [13] propose a set of features, including contextual features, registered atlas probability maps and an outlier map, to automatically segment MS lesions through a voxel by voxel approach. A rotation-invariant multi-contrast non-local means segmentation is proposed in [28] for the identification and segmentation of lesions from 3D MRI images. supervised learning by PSFM have been widely employed in tasks where the training database and the pre-selected feature set cover all possible cases [14]. Nevertheless, when the heterogeneity of the disease and the potential variability of imaging are large, as occurs for MS and MRI, the dimension of the training database and, mostly, the choice of the pre-selected features are critical.

AIPM do not require labelled training data to perform segmentation, but usually exploit some a-priori information, such as intensity clustering method, to model tissues distribution [74]. In [7], a likelihood estimator to model the distribution of intensities in healthy brain MR images is presented. Other methods use threshold with post processing refinement [56, 61] or are based on probabilistic models [29, 66]. A big hallenge for AIPM is that the outliers are not specific for lesions but could be due to artifacts, intensity in-homogeneity and small anatomical structures like blood vessels: this often produce false positives [11]. Moreover, AIPM are strongly based on the information extracted and simplified from the knowledge of specific experts.

Though the dimension of the training database is also crucial in DLM, these have no concern regarding the pre-selection of features as in PSFM or regarding a-priori information modeling as in AIPM.

In fact, during the last years DLM have gained popularity in medical imaging especially with CNN [41] and, in particular, with U-nets ad their variants [17, 45, 53, 79]. CNN, compared to machine learning approaches, achieved remarkable success in biomedical image analysis [11, 57, 68]. DLM train and learn themselves to design features directly from data [6] and provide best results in several problems, including the case of MS lesion identification/segmentation [4, 27, 33, 37, 71, 76]. This has also been confirmed in recent reviews [19, 21, 37, 75].

Some CNN employed for MS use 2D spatial convolutional layers [6, 58], others use 3D convolutional layers to incorporate 3D spatial information simultaneously [30, 54, 69, 70] and others merge spatial with temporal information to monitor disease progression over time [25, 59]. All these methods perform segmentation with a minimum lesion volume threshold to avoid the inclusion of small outliers.

However, CNN performance is still far from that obtained by human experts and, when they reach humans in some data sets, their performance dramatically drops with others [44]. In what follows we present

a framework based on CNN that can reach human performance in MS lesion identification/segmentation from WM

3   The proposed framework

The framework we propose, sketched in Figure 1, consists of the following steps: 1) deep learning automatic classification in three classes: Background, Uncertainty and Lesion (capital letter to imply the concept 'class'), optimized for Lesion (lesions from inside) and for Background (lesions seen in the context of the surrounding environment), separately for axial, coronal and sagittal sdirections (6 classificators result); 2) class fusion (separately for Lesion and Uncertainty, starting from Lesion) by performing the Union of the 2 axial segmentations (step 2a in Figure 1), followed by a majority vote used for confirmation of the class, by means of coronal and sagittal segmentations, elsewhere it is downgraded (step 2b in Figure 1); 3) final output.

   For the framework we propose, the following three hypotheses hold:

   1) input to the framework are the MSSEG pre-processed data from just one single MRI modality, FLAIR;

   2) the binary labelled ground-truth is revised to contain, besides Lesion and Background, also the Uncertainty class which is created by taking part of the original Background, and leaving Lesion unchanged, as described below;

   3) the three considered classes are supposed to be ordered, Background < Uncertainty < Lesion: as far as just Lesion and Uncertainty are the subjects of fusion, their downgrading consists in the passage from Lesion to Uncertainty and from Uncertainty to Background, respectively: Lesion is treated first to allow Uncertainty fusion to operate on the upgraded data set resulting from Lesion potential downgrading.

   Step 2a of Figure 1, serves to include, besides common information, also complementary information coming from the specificity of each of the two axial CNN and, in the same time, to model the reasoning of radiologists who use axial orientation to make first hypotheses. Step 2b is used to vote, for each object resulting from the axial processing (Lesion or Uncertainty), its permanence in the assigned class or its downgrading. Objects are confirmed when at least two of the other four raters (two coronal and two sagittal) agree with axial classification. This ensures that false positives are greatly reduced and that 3D contextualization with the environment is maintained. In this way, the model agrees with radiologist's reasoning regarding the usage of coronal and sagittal orientations to have a confirmation of the hypothesis and to better delineate the lesion borders.

   The choices regarding the usage of one single imaging modality, the classification in three classes and the use of an ensemble framework are clarified below.

   Being supervised, each classifier needs training, validation and test carried on by using data from a public data set. In what follows we first describe the used data set, the ternary ground truth, the CNN architecture, the used loss function, the hyper-parameters optimization and the ensemble, final, classification of Figure 1.

3.1   MSSEG data set

To allow a direct comparison and benchmark of the proposed framework with the state-of-the-art segmentation methodologies, we use the 2016 MSSEG data set [1]. In MSSEG, data were collected with several MRI scanners using different magnetic field strengths: 1.5T Siemens Aera, 3T Siemens Verio, 3T Philips Ingenia and 3T General Electric Discovery. The data set contains, for each examination collected in each scanner, T_1-w, T_1-w gadolinium enhanced (T_1-w Gd), T_2-w, T_2-FLAIR and PD-w images.

   We have chosen MSSEG because it includes 7 different classifications made by 7 different expert human raters, that makes it possible to compare our framework with human classifications, as well as with state of the art automatic strategies. For MSSEG, it was asked to the human raters to perform binary segmentation (each voxel was identified as lesion/not lesion): the annoted data set was composed by 15 training cases. Another subset of data, composed of 38 testing cases, was leaved without annotation. The training cases were accompanied by a consensus, a ground truth, calculated through statistical fusion (Lop-STAPLE) [3, 73] among the 7 manual segmentations.

   The images were made anonymous and furnished both in original form and pre-processed for user convenience.

   Preprocessing refers to a series of mathematical adjustments to MR images before segmentation [64] for reducing the effects of noise and imaging artifacts, equalizing space, eliminating outliers and stabilizing contrast. As previously stated, segmentation from MRI is difficult because of numerosity and
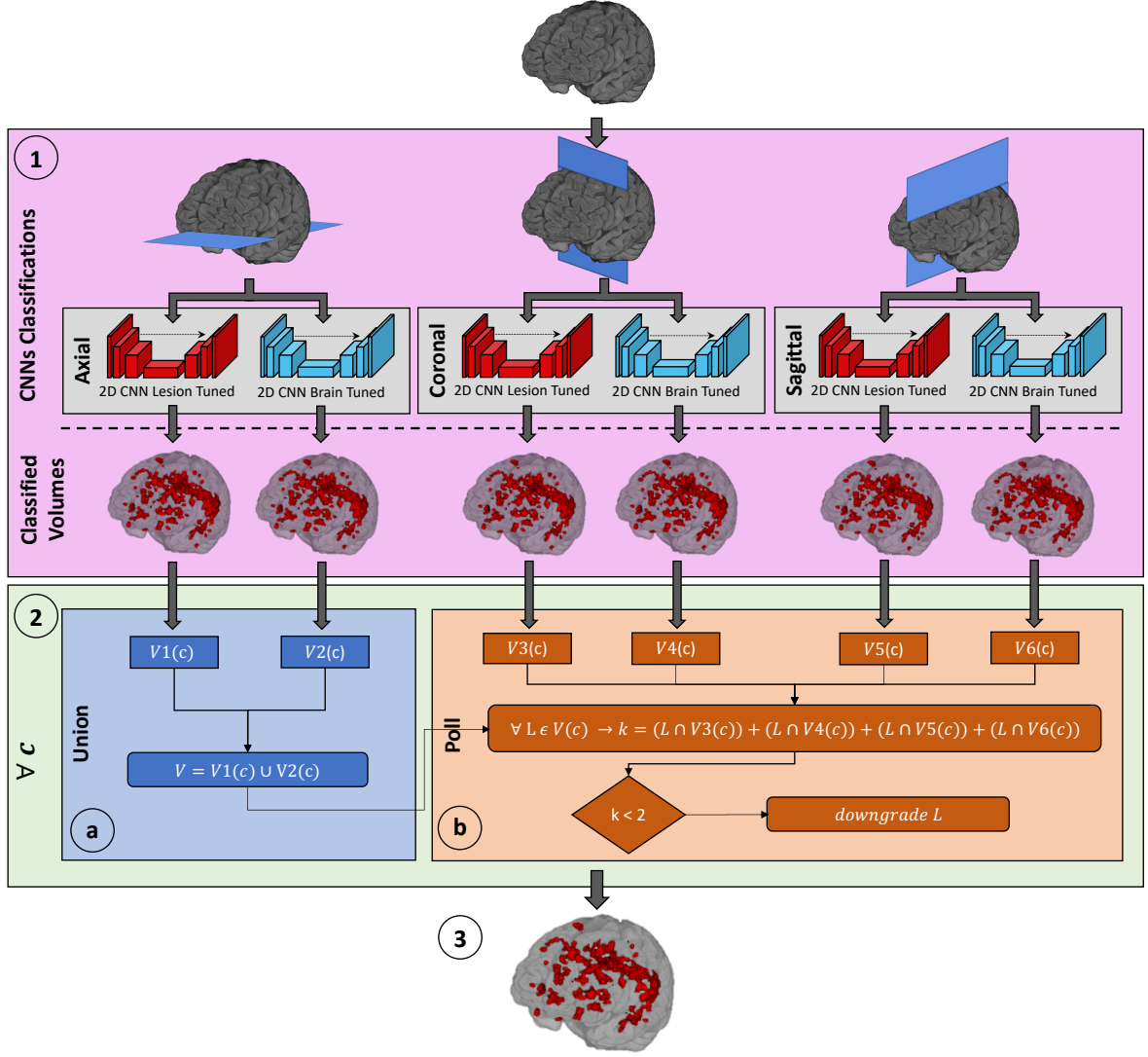
Figure 1: The proposed Identification/segmentation pipeline which divides brain tissue in three classes: healthy tissue (Background), tissue that has uncertain nature (Uncertainty), and MS lesions (Lesion). The strategy operates independently on axial, coronal and sagittal volumes, each consisting of two separately trained U-nets, one optimized on Lesion, for searching lesions from their inside, and the other optimized on Background, for contextualizing lesions them with respect to the environment. After that, it recombines the results by using the Union of axial volumes and by using a majority voting strategy on the coronal and sagittal volumes, for confirmation. Voxels whose classification is not confirmed are downgraded (Lesion becomes Uncertainty and Uncertainty becomes Background. The framework operates separately for Lesions and Uncertainty, starting from Lesion. In step 2b, the procedure is applied voxel by voxel: L is referred to each single voxel of the class $c \in \{Lesion, Uncertainty\}$.

variability of parameters, overlapping intensities, noise, gradients, motion, blurred edges, anatomical variations and susceptibility artifacts [9, 50]. For this reason, images undergo pre-processing to allow image stabilization, to make classification more robust with respect to imaging and scanners. Standard pre-processing consists on: noise reduction, volume registration and alignment, bias field correction, skull stripping and contrast normalization through z-score. However, though reduced, some imaging variability remains mainly depending on the specificity of the used imaging sequences. This could be a problem for an automated strategy which use more than one single imaging modality. Indeed, little variations in each single imaging modality could correspond to huge variations in their concatenation, thus resulting in a drop of performance when changing data set [44]. In our framework we opt for the usage of one single modality, FLAIR, the most informative one to detect/segment MS lesions in WM,

5

to demonstrate that a single modality could be sufficient for MS lesion identification/segmentation from WM; to avoid that the potential gain of using multiple imaging modalities could be overcome by the drop in robustness and performance due to residual MRI instabilities after pre-processing.

Though a specific pre-processing step for local contrast normalization of FLAIR images has recently been proposed [51], we use FLAIR data as pre-processed in MSSEG to: 1) easily distinguish the advantage the proposed framework really has with respect to other automated frameworks; 2) compare the proposed framework with human experts for whom additional pre-processing was unavailable.

Further, we divide annotated MSSEG data set, composed by 15 subjects, in three subsets respectively for training, validation and test, as follows:

the training data set contains examinations from 9 subjects, 3 subjects of each center;

the validation data set contains data from 3 subjects, one for each center;

the test data set contains the remaining data, from 3 subjects, one for each center.

The examinations are swap and an exhaustive cross validation is performed while maintaining the proportions between centers. Once the data set is established, it is augmented by adding, for each image, 2 random rotations (between -13 and 13 degrees, 1 degree in resolution), 1 random scaling (between 1.1 and 1.3, 0.01 in resolution) and 1 gaussian random noise addition, 0 mean and 0.001A variance, where A is the maximum amplitude value in the examined volume.

The augmented data set, for each swap and orientation (axial, coronal and sagittal), contains 5216 images for training, 418 images for validation and 435 images for test.

3.2   Ternary ground-truth

In medical imaging it is often made the simplifying assumption that there is a single, unknown, true segmentation map of the underlying anatomy, and each human rater produces an approximation with variations reflecting individual experience with respect to the problem. The concept of a single-truth assumption may be correct when assuming that there exists only one (true) boundary of the physical objects captured in an image and ambiguities in interpretations are due to human mistakes and disagreements.

In the opposite case, it can be assumed that variable annotations from experts are all realistic and acceptable instances of the true segmentation.

As often occurs, the true is in the middle i.e., some ambiguities are indeed specific to human subjectivity or imperfections (extrinsic) while some are due to the problem itself (intrinsic). In our problem, both are important but intrinsic ambiguities have the highest role, being due both to MS presentation and to MRI not specificity: lesions are not well separated from healthy tissue in MS (PVE) and MRI is neither sufficiently specific for MS nor sufficiently precise, as discussed above. Regarding human subjectivity, this produces differences that are due to a mix of prior assumptions, experience in the field, more or less exploitation of additional meta-information (such as anatomical/radiological/clinical knowledge), mistakes or oversights which often are concentrated on small and/or low intensity lesions and lesion borders.

When raters are forced to furnish a binary segmentation, as in MSSEG, they cannot express any doubt, whatsoever is the cause. Binary segmentation does not allow the representation of intrinsic uncertainty but, further, induces a human rater to assume polarized decisions which, from one side, could not correspond to what the rater really believes and, from the other side, could confuse and mislead an automated strategy during training. In fact, ambiguous decisions could have been assumed by the rater in similar situations (an uncertain region could be considered healthy tissue in one case and lesion in another).

However, we have to cope with just binary classification from human raters. If we want to teach an automated method that an intrinsic uncertainty is present in the problem, we need to integrate the binary ground-truth with human uncertainty (doubts), and to make it robust to out-of-training-set examples, in particular the ability to develop robustness to adversarial examples [40, 49], as those deriving from MRI and MS. However, to maintain the possibility of comparing different strategies on the same ground-truth, we don't want to completely redefine it [27, 35, 36], but to consider as uncertainty what at least two of the seven human raters of MSSEG have considered as lesions, though the binary consensus has not. In this way, we don't touch the Lesion of the binary consensus but we create space for Uncertainty from Background.

The method we propose is quite different from other strategies used to define uncertainty [27, 35] and it has the following motivations: 1) to maintain the original structure of the lesion consensus. In fact, to date, STAPLE and its derivations are considered the best strategies to calculate, by the segmentation
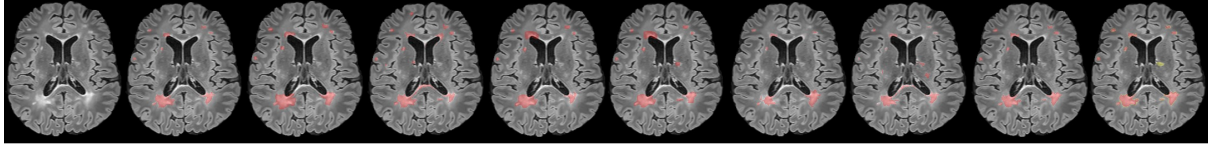
Draft

Figure 2: A sample FLAIR image from the 2016 MICCAI data set (left) and the binary classifications from the 7 human raters (middle). The last two columns report the binary consensus and the proposed ternary consensus, respectively. Lesion is annotated in red. In the ternary consensus, Uncertainty is annotated in yellow.

of a set of raters, both a probabilistic estimate of the true segmentation and, at the same time, a measure of the performance for each rater with respect to the unknown ground truth [3, 35, 36]. 2) to account for the uncertainty affecting both the problems and the raters, by considering as uncertain those regions which at least two raters considered Lesion, though these were leaved out from the binary consensus. 3) to avoid that the Uncertainty could affect the Lesion of the original MSSEG consensus, thus allowing a direct comparison with other methods. 4) to quantify the gain the proposed framework could effectively get when uncertainty is introduced with respect to its absence. 5) to allow the learning strategy to consider as uncertain not only lesion borders, as other Authors do [35], but also whole regions not necessarily connected to lesions. In fact, the uncertainty could regard both lesion borders, where damaged tissue could coexist with healthy tissues (PVE), but also whole structures, where doubts are due to MRI unspecific nature for MS.

Fig.2 reports an example FLAIR image with the seven human binary classifications, the binary consensus and the proposed ternary consensus. Uncertainty, in yellow in the ternary consensus (last image on the right), indicates doubtful regions where discordant decisions are assumed by raters but where at least two raters agree. The resulting ternary consensus is used as ground truth to train our framework in reaching a ternary classification.

3.3 CNN architecture

The task we are facing with is the classification of each voxel of a FLAIR volume, separated into slices, in one of the three slices: Background, Uncertainty and Lesion. Since U-nets [53] are specifically designed for these tasks, in this work we use the U-Net architecture depicted in Figure 3.

The U-Net is a fully convolutional neural network composed by 2 main sections, Contraction and Expansion, connected by a Bottleneck section. Corresponding Contraction and Expansion modules are also connected through skip connections.

Compared to the traditional U-net architecture, we insert a batch normalization layer in each block to mitigate the effects of gradient amplification [60] in regions surrounding the lesions, though with a relevant increase of computational costs (about 30%).

An important parameter for a U-net is the number of blocks in Contraction and Expansion sections. If the number of the blocks is too low, the network could not have enough features for learning complex structures. On the other hand, if the number of the blocks is too high, the network memorizes complex structures and overfitting occurs.

To optimize the number of blocks n, we performed some preliminary training, with $n \in \{3, 4, 5\}$. We did not go outside this set because for $n = 5$ the U-Net started to overfit, even when using high values of L_2-Regularization, and for $n = 2$ a dramatic drop of performance occurred. With $n = 4$, the problems related to overfitting disappeared and the performance was good. However, we noticed from the feature maps that some redundancy was present. For this reason, we trained the CNN with $n = 3$ and verified that redundancy was greatly reduced and training converged faster than for $n = 4$: hence, $n = 3$ is the number of blocks used thereinafter.

3.4 Loss function and process optimization

The CNN we use have to solve a three class automatic annotation, for which a Multi-label Cross Entropy Loss Function is necessary. We use the following:
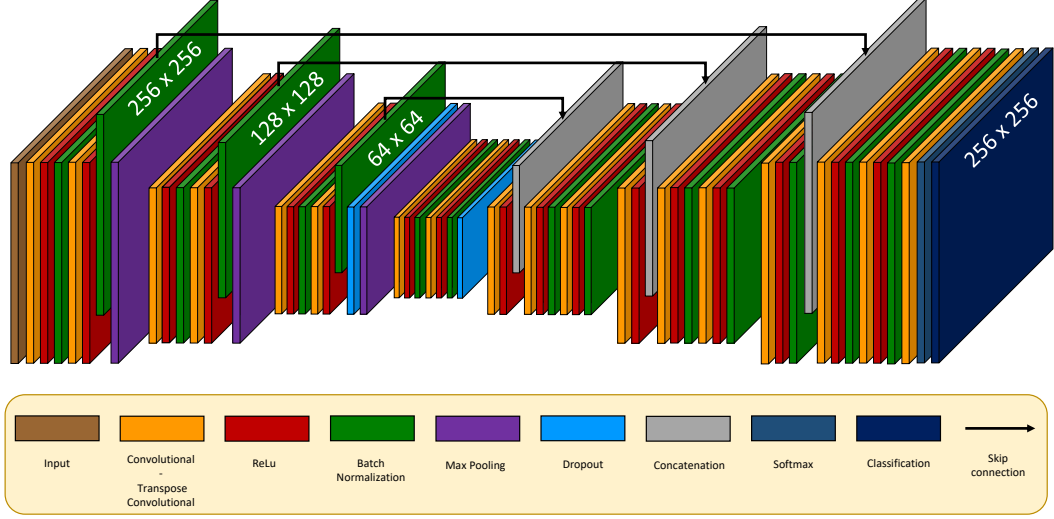
Figure 3: The used U-net architecture. The architecture is the same for 6 classifiers, though they have been trained separately.

$$loss = \frac{1}{N} \sum_{n=1}^{N} \sum_{i=1}^{K} (T_{ni} log(Y_{ni}) + (1 - T_{ni}) log(1 - Y_{ni})) \tag{1}$$

where N and K are the numbers of observations and classes, respectively.

The use of three classes, besides problem stabilization (the presence of the Uncertainty class gives better confidence in defining both lesions and background), allows also to consider another important aspect. Indeed, we can optimize two CNN, sharing the same architecture and the same loss function (Eq.1), but with a different learning process deriving from different focus: one optimized on Lesion and the other on Background (the environment in which lesions are immersed). The middle class, Uncertainty, is used as a sort of "*buffer class*". In a binary classification problem this would not have been possible: the optimization of one would automatically lead to the optimization of the other (what is not Lesion is Background and vice-versa). The usage of Uncertainty gave to both CNN a new choice to break that constraint.

The training process of a neural network can be controlled by hyper-parameters. Different hyper-parameters lead to a different learning path and, finally, to different performance of the neural network. In literature, it is well known that the hyper-parameters optimization serves to achieve faster training and better performance [8, 31, 77]. In this work hyper-parameter optimization is also used to train the two CNN separately which leads to different paths discovered by the Gradient Descent.

The hyper-parameter setting is driven by automatic optimization through a Bayesian approach [63]. In this work the chosen hyper-parameters to be optimized are:

1. **Starting Learning Rate**: it is related to the data set and to the type of neural network.

2. **L2-Regularization**: it prevents overfitting.

3. **Class balancing**: it optimizes the amplification factor for the represented classes and improves training (here we have three classes, hence two weights are sufficient (Lesion Weight and Background Weight).

Of the above, the first two are standard for CNN, while Class balancing is specific for our CNN because it helps to differentiate the path of optimization between the CNN optimized with respect to Lesion and that optimized with respect to Background.

The resulting optimization problem is the following:

8

Table 1: The hyper parameters values for the CNN, each trained with the corresponding oriented images. Suffixes In and Out are used to indicate the CNN in which Lesion is optimized (In) or Background is optimized (Out).

CNN	Learning Rate	L2-Reg.	Lesion Weight	Background Weight
Axial In	5,32E-04	3,66E-10	7,98E-02	8,91E-01
Axial Out	4,54E-04	1,14E-10	2,99E-02	9,00E-01
Cor. In	6,50E-04	3,66E-10	7,98E-02	8,71E-01
Cor. Out	3,18E-04	7,92E-09	6,59E-02	8,58E-01
Sag. In	1,01E-04	5,53E-09	7,01E-02	8,74E-01
Sag. Out	1,08E-04	3,41E-09	6,02E-02	8,50E-01

$$x^* = argmin_{x \in X} f(x) \qquad (2)$$

where X is the domain of x, $f(x)$ represents an objective function to be minimized and x^* is the hyper-parameters setting that yields the optimal value of $f(x)$.

In this work $f(x)$ is defined as

$$f(x) = 1 - IoU(x) \qquad (3)$$

where IoU is the Intersection over Union score [21] defined in Section 4.

Regarding the two CNN used therein, for that optimized for Lesion, the IoU is calculated with respect to the Lesion class and, for that optimized for Background, the IoU is calculated with respect to the Background class.

Table 1 reports the hyper parameter setting for both the optimized CNN ('In' and 'Out' indicate Lesion optimization and Background optimization, respectively) for each direction (axial, coronal and sagittal). As can bee observed, the overall change of the hyper parameter setting justifies different training paths for the CNN and different points of convergence for each of them.

3.5 Ensemble Classification

It is well known that ensemble classifiers often perform better and more robustly than its single components [12, 18]. For the classification of lesions we use 2D slices (axial, coronal and sagittal) of the whole volume, with specific CNN trained separately with axial, radial and sagittal slices, respectively. In this way, we can avoid that a particular orientation could be favourable to lesions (the classifier is deceived) or to the classifier (the good classification of some lesion could be a lucky outcome). Further, it serves to ensure 3D continuity to the classification. Moreover, as explained above, we look lesions both as themselves and with respect to the surrounding environment.

We obtain a set of 6 classifiers, two for each of the three orientations, axial, coronal and sagittal, whose classification has to be to merged to produce a single output resembling radiologists reasoning: though 3D FLAIR data are collected following sagitall planes to account for clinical/physical issues, radiologists often use axial images for data interpretation and use the other orientations for confirmation [22, 67]. Accordingly, we prefer axial classifications and use coronal and sagittal output for confirmation.

Regarding axial classifications, since each of the two CNN referred to the same direction insist on the same scenario but with different approaches, they collect specific information in those regions where reasoning is specific. Since both specific contributions are important, besides common findings, a Union operation between the two classifications is required. Other forms of fusion, for example statistical fusion

Draft

through STAPLE [35, 36, 73], are inappropriate because in our case we are combining classifications obtained by different approaches and not classifications from similarly reasoning raters (where it is supposed to use almost the same approach). Regarding this last point, it is important to notice that also human experts with different experience could assume different decisions [47].

However, being the classified volume a three values data set, Union does not correspond to the classic binary union operation. In our case, Lesion is privileged, then comes Uncertainty and, finally, Background. In fact, a voxel is classified in a lesion if at least one of the two classifications considers it as a lesion; elsewhere, it is classified Uncertainty if at least one of the two classifications consider it as uncertain; elsewhere, it is considered Background (both classifications affirm the voxel is Background).

After Union application, false positives are present more than each single classifier: their number is reduced by using the majority vote between the other 4 classifications (two coronal and 2 sagittal, all compared along axial planes). In fact, for each voxel the class is maintained if at least two of the other classifiers confirm it, elsewhere it is downgraded by one (a potential Lesion becomes Uncertainty, a potential Uncertainty becomes Background): a double step is not allowed. There is always at most 1-step downgrading at once. This means that first a decision is made on Lesion and, then, on Uncertainty by using the data set resulting from the application of the process to Lesion.

The ensemble of different classifiers is justified both by the fact that Union has to join common information, as well as specific information from each of the two axial classifiers, and because each potentially positive voxel needs confirmation from the coronal and sagittal classifiers (in this case, also 3D spatial information is considered). Though we don't have measured the diversity degree between classifiers [39] we have preferred to resemble the usual procedure used by radiologists and to rely on the usual benefits of using an ensemble classifier [12].

We have copied the human behavior in the proposed automatic pipeline by privileging axial sections with respect to the others, but we also performed trials regarding the preference of the other orientations in the fusion process and the results, not shown, confirm that axial preference gives the best results, closely followed by coronal and, at a great distance, by sagittal, though it is the direction used for 3D FLAIR data collection. This could be explained, at least partially, by the fact that axial and coronal slices show highly symmetrical shape both regarding brain anatomy and lesion shapes, also across different subjects, thus making learning process easy. This is not true for sagittal directions, in which symmetry is absent and to a little rotation of the head could correspond a huge variation of the image content.

4   Evaluation Metrics

In the binary classification problem the voxels are positive (P), Lesion, and negative (N), Background. In a ternary ground-truth, P represents the voxels of the class we are considering at present (Lesion or Uncertainty), while N represents the negative voxels (those of the two classes not considered at present). According to this definition, for a given rater the same relative rules hold (with respect to the class considered at present): TP are the true positive voxels, TN are the true negative voxels, FP are the false positive voxels and FN are the false negative voxels. Having the considered class fixed, a voxel can be just one between TP, TN, FP and FN.

As far as we need an exhaustive comparison between all the raters involved therein (artificial, single humans and ground truth) and that a unique performance parameter is unavailable, we define and calculate all the mostly known metrics. In what follows, we define all the used metrics by separating those oscillating in in the interval $[0, 1]$, whose ideal value is 1, by those oscillating in the interval $[0, \infty)$, whose best value is 0. The two groups are distinguished for graphical purposes. For more details about the reported metrics, please refer to [15, 19–21, 72].

4.1   Metrics convergent to 1

Sensitivity (also called recall or true positive rate) is defined as:

$$SENS = \frac{TP}{TP + FN} \tag{4}$$

The sensitivity measures the portion of positive voxels that are correctly identified. In this problem, the sensitivity measures the capabilities of a method to correctly classify the voxels labelled as allowing to the desired class, without underestimation. In fact, sensitivity values range between 0 ($TP = 0$) and 1 (when $FN = 0$). We also distinguish an object sensitivity, $OSENS$, defined as:

$$OSENS = \frac{TP_o}{TP_o + FN_o} \tag{5}$$

in which the subscript o indicates we are referring to whole objects and not to single voxels. An object is considered as TP if the intersection with the corresponding object in the ground truth is not empty.

Specificity, also called true positive rate (TPR), is defined as:

$$TPR = \frac{TN}{TN + FP} \tag{6}$$

TPR represents the portion of negative voxels N that have been correctly identified. For the treated case, since classes are strongly unbalanced, TPR is biased by the fact that most of the image surface is covered by negative voxels: for this reason high specificity does not guarantee good performance (we reported it for completeness).

Accuracy (ACC)is defined as:

$$ACC = \frac{TP + TN}{P + N} \tag{7}$$

but, due to unbalancing, we use the following normalized ($ACCN$) definition:

$$ACCN = \left(\frac{TP}{TP + FN} + \frac{TN}{TN + FP} \right) /2 \tag{8}$$

to make it more representative.

Positive Predicted Value (PPV), also called Precision, is defined as:

$$PPV = \frac{TP}{TP + FP} \tag{9}$$

PPV represents the portion of voxels identified as positives which are really positives (TP). PPV measures how the method correctly classifies voxels in the correct class without overestimating the class itself. In fact, PPV ranges between 0 (TP=0) and 1 (FP=0).

As for $OSENS$, we have defined an object-based PPV, $OPPV$, as follows:

$$OPPV = \frac{TP_o}{TP_o + FP_o} \tag{10}$$

in which the subscript o indicates we are referring to whole object, as above. $OPPV$ represents the portion of objects identified as positives which are really positives (TP_o). $OPPV$ has the same meaning of PPV but for whole objects and not for single voxels.

Correct Detection Ratio (CDR) is defined as:

$$CDR = \frac{TP}{MSA} \tag{11}$$

where MSA is the manually segmented area (in our case it corresponds to all the voxels in the ground truth allowing to the considered class).

Dice score, also called Sorensen–Dice coefficient, is defined as:

$$Dice = \frac{2 * TP}{2 * TP + FP + FN} \tag{12}$$

$Dice$ score measures the similarity between two data sets. This index is widely used in AI for validation of image segmentation algorithms. In the text we refer to Dice score as Global Dice score to distinguish it from Image Dice score.

Image Dice score uses the same equation of Global Dice score but, while Global Dice score is calculated on the whole data set, Image Dice score is applied on each single image and finally averaged on the number of images. Image Dice score allows to the so called per-image metrics [20]. Per-image metrics are important because they tend to highlight local behaviour.

A score similar to $Dice$ is the Intersection Over Union (IoU):

$$IoU = \frac{TP}{TP + FP + FN} \tag{13}$$

11

where the difference is in the weight of TP.

The $F1$ Score (calculated for whole objects and not for single voxels) is defined as:

$$F1 = 2 * \frac{OSENS * OPPV}{OSENS + OPPV} \tag{14}$$

where $OSENS$ and $OPPV$ are defined above.

BF score is a per-image version of $F1$ score.

Pearson Correlation Coefficient (PCC), between two data sets A and B, is defined as:

$$PCC(A, B) = \frac{cov(A, B)}{\sigma_A * \sigma_B} \tag{15}$$

where $cov(A, B)$ is the covariance of A and B and σ_A and σ_B are the standard deviation of A and B, respectively. PCC can range in the interval $[-1, 1]$ and a negative value of PCC indicates a similarity of the object A with the negative version of the object B.

4.2 Metrics convergent to 0

The following metrics are those in which the ideal value is 0. In what follows we report those used in the present manuscript.

Extra Fraction (EF), is defined as:

$$EF = \frac{FP}{TP + FN} \tag{16}$$

Detection error rate (DER) is defined as:

$$DER = \frac{DE}{MTA} \tag{17}$$

where DE is the detection error over the mean total area (MTA). DER measures the disagreement in detecting the same regions between the current rater and the ground truth. Outline Error Rate (OER) is defined as

$$OER = \frac{OE}{MTA} \tag{18}$$

where OE is the outline error over the MTA. OER measures the disagreement in outlining the same object between the evaluated method and the ground truth.

False Detection Ratio (FDE) is defined as:

$$FDE = \frac{ASA - TP}{MSA} \tag{19}$$

where ASA is the automatic segmented area.

Relative Area Error (RAE)is defined as:

$$RAE = \frac{ASA - MSA}{MSA} \tag{20}$$

Hausdorff Distance (HD) between two objects A and B is defined as:

$$HD(A, B) = max(h(A, B), h(B, A)) \tag{21}$$

where $h(A, B)$ is:

$$h(A, B) = max_{a \in A} min_{b \in B} \parallel a - b \parallel \tag{22}$$

HD measures how far two subsets are from each other. In other words, two sets are close with respect to HD if every point of one set is close to some point of the other set.

Euclidean Distance (ED) between two objects A and B is defined as:

$$ED(A, B) = max(d(A, B), d(B, A)) \tag{23}$$

where $d(A, B)$ is defined as:

$$d(A, B) = \frac{1}{N} \sum_{a \in A} min_{b \in B} \parallel a - b \parallel \tag{24}$$
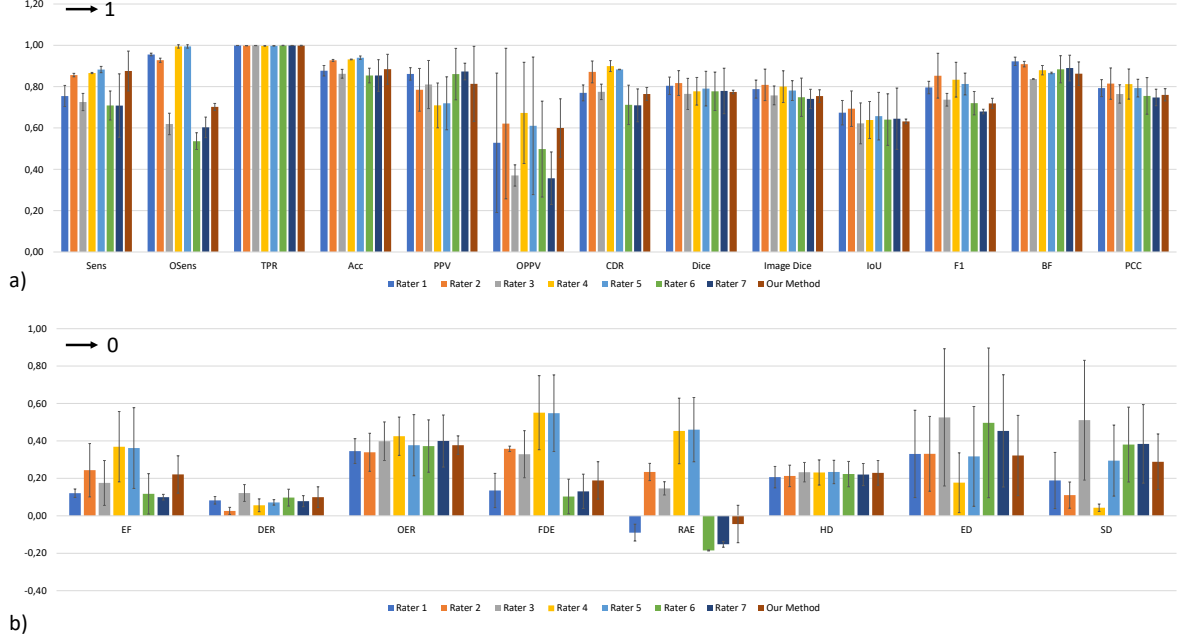
12

Figure 4: Comparison between the raters and the ground truth, performed on Lesion. The reported metrics are separated in those whose ideal value is: 1 (a) and 0 (b). Average and standard deviation are reported. Euclidean, Hausdorff and Surface distances are shown in cm units.

Surface Distance (SD) is defined as:

$$SD = \frac{\sum_{i \in A_S} d(x_i, G_S) + \sum_{j \in G_S} d(x_j, A_S)}{N_A + N_G} \qquad (25)$$

where A_S and G_S are two segmentations (one is the rater segmentation and the other is the ground truth), d denotes the minimal ED between voxels on both surfaces and N_A and N_G denote the number of points of each surface.

5   Results and Discussion

The proposed framework is trained, validated and tested on the ternary consensus defined above. As far as the ternary consensus maintains unaltered all the lesion voxels allowing to the original MSSEG binary consensus, we can guarantee a direct comparison with human raters who furnished binary segmentation and, at the same time, with existing automated methods tested on the same data set. Regarding the segmented Uncertainty, a comparison is possible just with respect to the ternary ground-truth, since for the human raters Uncertainty is unavailable. In principle, we could have force the definition of Uncertainty for each rater by considering as uncertain the voxels that the rater did consider Lesion and the binary ground-truth did not. Though we made some experiment in this direction, we believe this comparison should deserve a specific and deep discussion, being it based on approximated hypotheses (the intention of each rater would be guessed, not real), which is out the scope of this manuscript.

The evaluation of all the raters, the proposed framework and the human radiologists, both with respect to the ground-truth and with respect to each-other, is performed by applying the cross-validation approach defined in Subsection 3.1. Average and standard deviation values are calculated for the metrics defined in Section 4 and divided in two groups: those whose ideal value is 1 and those whose ideal value is 0.

The first results, reported in Fig 4, are those between the raters and the ground-truth performed on the class Lesion. This is also an indirect comparison, consensus mediated, between the proposed framework and the human raters. For a better overview, the mean values are also shown in Fig. 5 by using a radar visualization: they confirm that the behaviour of the proposed method is between the inter-rater variability.
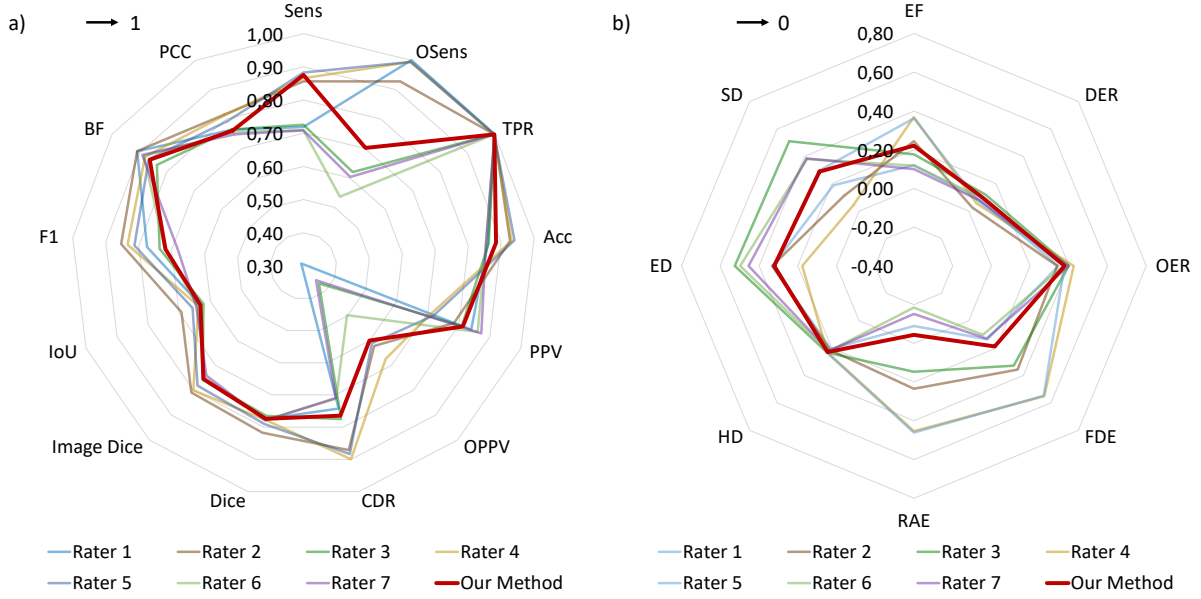
13

Draft

Figure 5: Comparison between raters in the same conditions of Fig. 4. Fro graphic purposes, just the average is reported for each metric and the line of the proposed framework is highlighted.

As can be observed, our framework is never the best or the worse, for at least one of the metrics, as instead occurs for human raters. This can be explained, at least partially, by the fact that it has been trained with the consensus that, for its nature, tends to average pros and cons of the raters from which it has been derived.

A Wilcoxon signed-rank test of the vectors of metric values confirms, with a significance level of 0.01, that there is no significant difference between the behaviour of our method and that of the 7 human raters, with respect to the ground-truth, on the Lesion class. This means that, if data are shown without labels, it would be impossible to recognize the automated rater from humans.

As far as lesion size could greatly affect the performance of the classification [19] and the previously reported results are averaged with respect to lesion volume, we repeat the comparison by differentiating with respect to lesion volume. To this aim, we consider all the lesions separately and the calculations are performed lesion by lesion, by maintaining separated also lesions of the same volume. In this way we can: 1) visualize potential outliers; 2) represent lesion density; 3) avoid local averaging that could mask specific contributions to the metrics. The results, reported just for the most commonly used metrics [19], are shown in Fig. 6.

Results again confirm the analogy of behavior between the proposed framework and the 7 human raters, though for some volumes our framework exhibited results close to the borders of oscillation of the 7 human raters. Indeed, a greater dispersion can be observed for F1-score and a relatively high average value is observable for SD, though in line with that of some human rater.

Though the above good results, it does not mean that our framework behaves like human raters because the comparison is mediated by consensus. In other words, our framework could be at the same 'distance' as the human raters from the ground-truth, but on the opposite side. For this reason, a direct comparison is necessary to finally confirm the similarity between the proposed framework and the human raters. To this aim, we perform the experiment of comparing all the raters to each other by considering ground-truth all of them, including our framework, in rotation. Results, for the most frequently used metrics, are reported in Fig. 7.

These results unequivocally confirm that the proposed framework's behaviour does not differ from that of the other human raters and that it is not polarized toward a specific rater or toward the consensus. Moreover, as also other Authors highlighted [27], results also show that manual segmentation from some human raters (R4 and R5) are almost the same but they are quite dissimilar from those of the other human raters. Fortunately, results also confirm that the MSSEG consensus is not biased by the similarity between raters R4 and R5 and that it maintains a "human" role, though it is created as a consequence of a "mediation process". In fact, the MSSEG consensus shows very similar behaviour to human raters

Draft
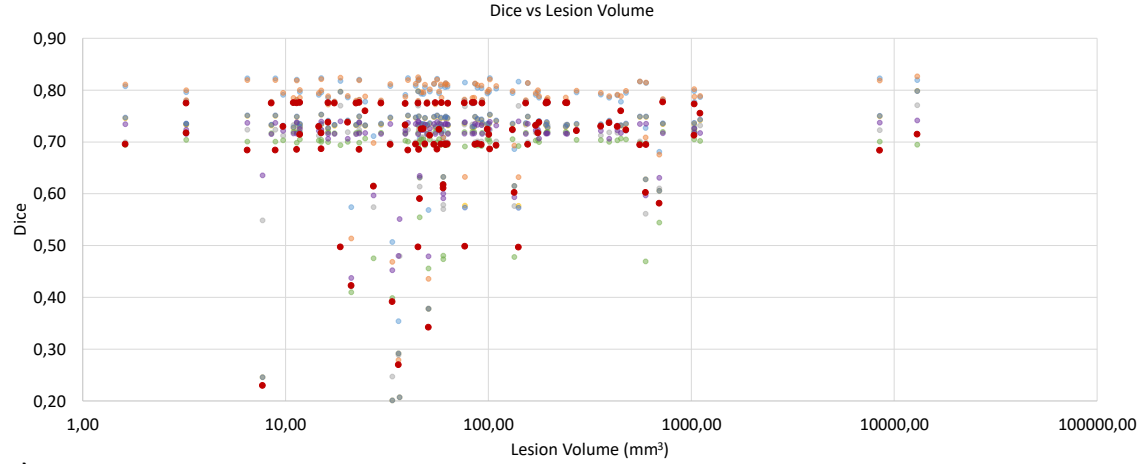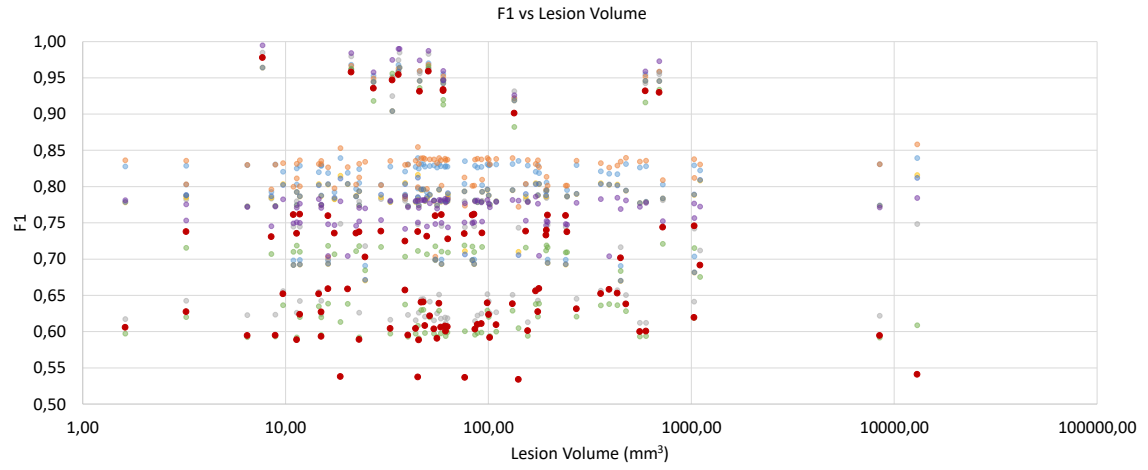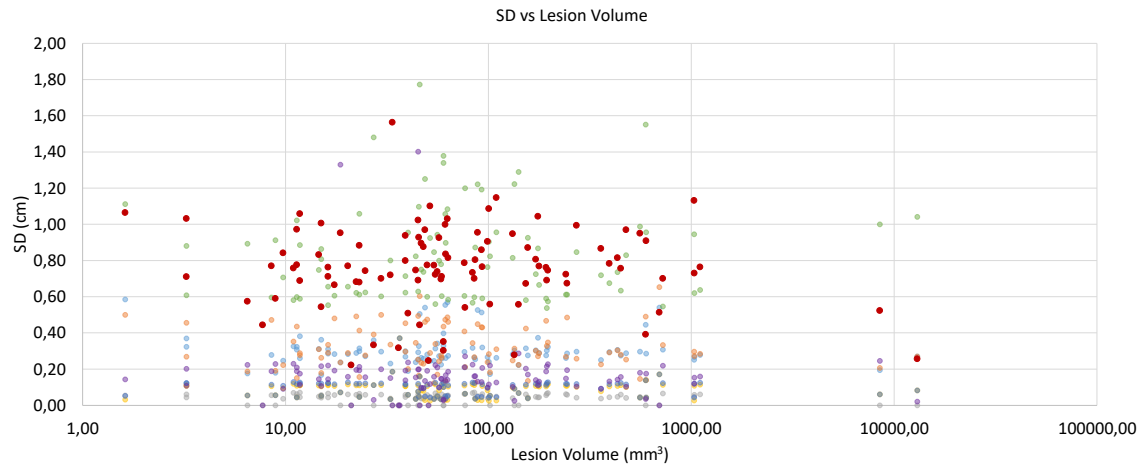
Figure 6: Dice score (a), F1-score (b) and Surface Distance (c), calculated for each lesion and shown with respect to the lesion volume for the human raters and the proposed framework. To improve readability, the logarithmic scale is used for lesion volume and framework's values are highlighted.
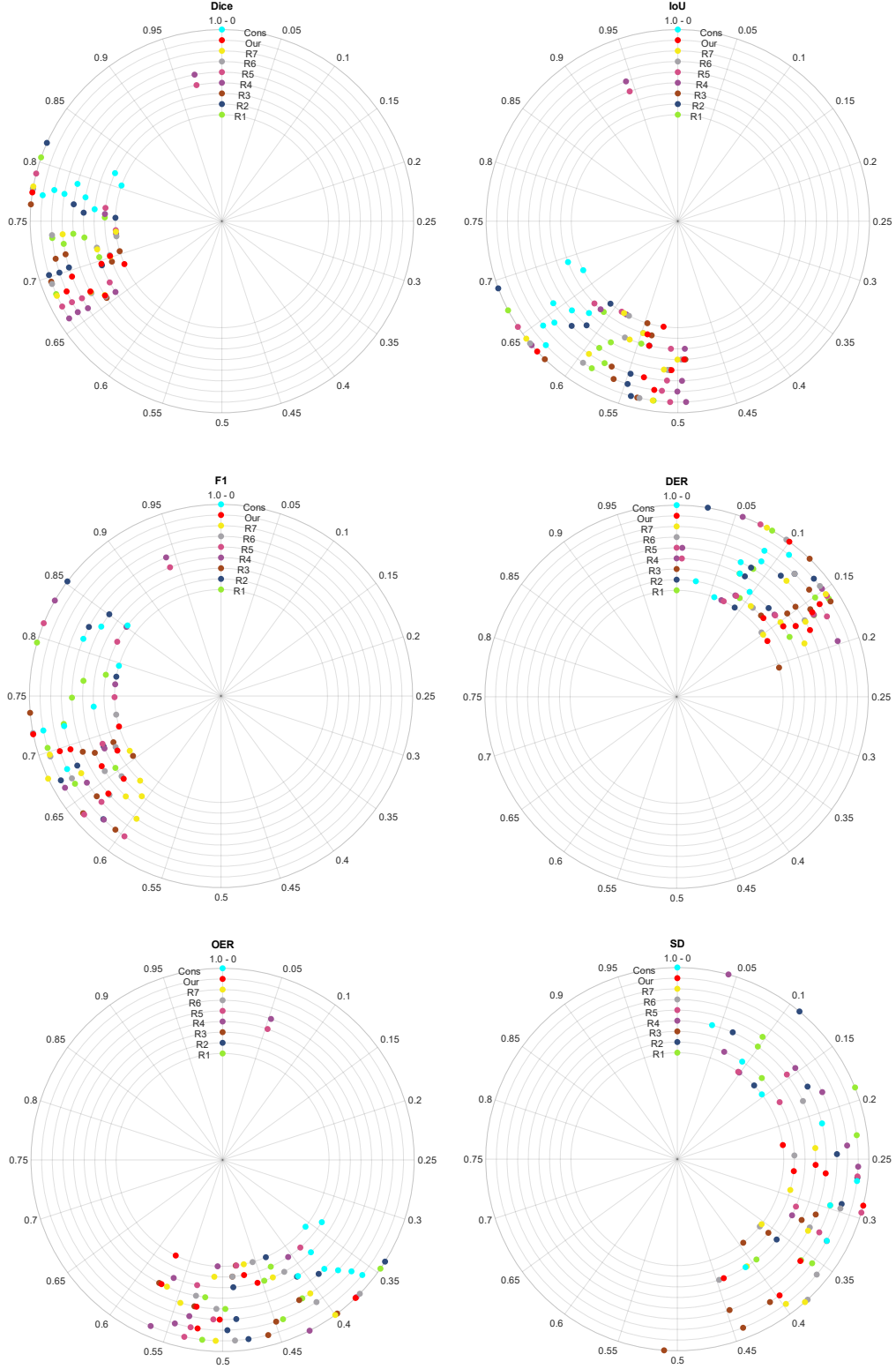
15

Draft

Figure 7: Comparison between all the raters with respect to each other, including our framework and consensus, each alternately considered as the ground-truth. For readability purposes, only some metrics are reported. In this representation, angular position indicate the metric value: radial information serves just to separate the current ground-truth rater. Ground-truth raters have colored bullets placed on the vertical line to indicate 1 for metrics converging to 1 and 0 for metrics converging to 0. This representation places together metrics converging to 1 and to 0: clock wise versus for metrics to 1, anti-clock wise versus for metrics to 0.
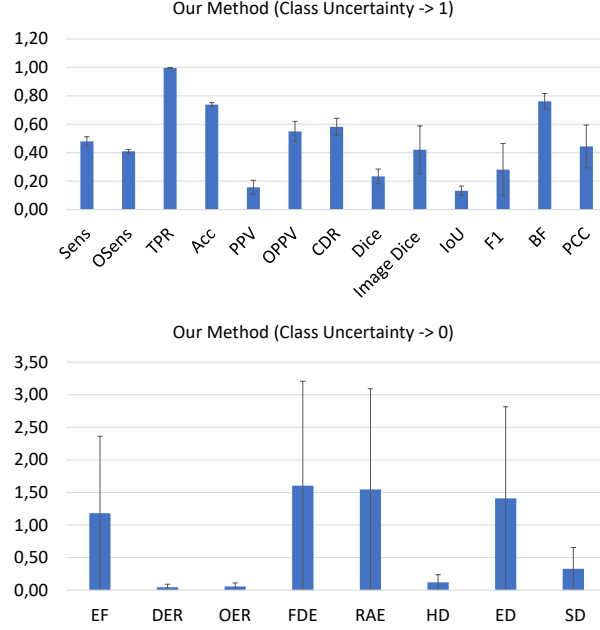
16

Figure 8: Average and standard deviation values of the metrics calculated for Uncertainty with respect to the same class in the ternary ground-truth. Values are separated between those converging to 1 (a) and those converging to 0 (b).

R1 and R2. This is a fundamental aspect because it means that all the people who are attempting to train automated systems with respect to the MSSEG consensus, including ourselves, are not following a "chimera" to which, paradoxically, the closer we get, the more we move away from the proper objective.

As far as we have confirmed the good performance of the proposed framework regarding Lesion, we now pay attention to the Uncertainty class, that the proposed framework has also learned and classified. To this aim, Fig. 8 reports average and standard deviation values for the metrics calculated with respect to the corresponding class of the ternary ground truth. If compared with the values obtained for Lesion, results are very poor, especially for metrics whose ideal value is 1. However, the 3D annular shape exhibited by Uncertainty around lesions, which includes two borders (external and internal) often discontinuous, greatly contributes to lower the results. Moreover, we don't have human references for Uncertainty and, for this reason, a comparison is impossible. Hence the results for Uncertainty are just reported for completeness and future comparison.

A visual overview of the behavior of the proposed framework in the whole process of identification/segmentation, both for Lesion and for Uncertainty, with respect to the ternary ground truth, is shown in Fig. 9. The ternary ground-truth is reported on the left side, the corresponding segmentation obtained with the proposed framework is presented on the right side, for the same subject and slices. Both for Lesion and Uncertainty, the proposed framework selects more than necessary (FP are evident). Interesting is the almost absence of FN in the segmented volume. The other interesting propriety shown by the proposed framework is the good spatial continuity of the lesion structures in the 3D model of Lesion (upper right panel). Lesion is annotated in red, Uncertainty is annotated in yellow.

To complete our discussion, it remains to compare the proposed framework with recently proposed automated strategies. To this aim, Table 2 contains this indirect comparison on the metrics calculated for at least one of the other methods. The necessary condition for a method to be considered in Table 2 is to have been trained, validated and tested on the 2016 MSSEG data set. In this way, we can ensure that the comparison is homogeneous and performed on the same conditions of that obtained with respect to the 7 human raters.

Though a global ranking is difficult, data reported in Table 2 are clear: the proposed framework is the most stable with respect to different metrics and it generally outperforms the other methods, including those methods which use multiple imaging modality. This could have an interesting implication: as the automated framework performs like human raters just using FLAIR, it means that FLAIR would contain sufficient information, not only necessary, to identify and segment all MS lesions occurring in the WM, independently of their status. Positive consequences could be: a) due to the huge variability
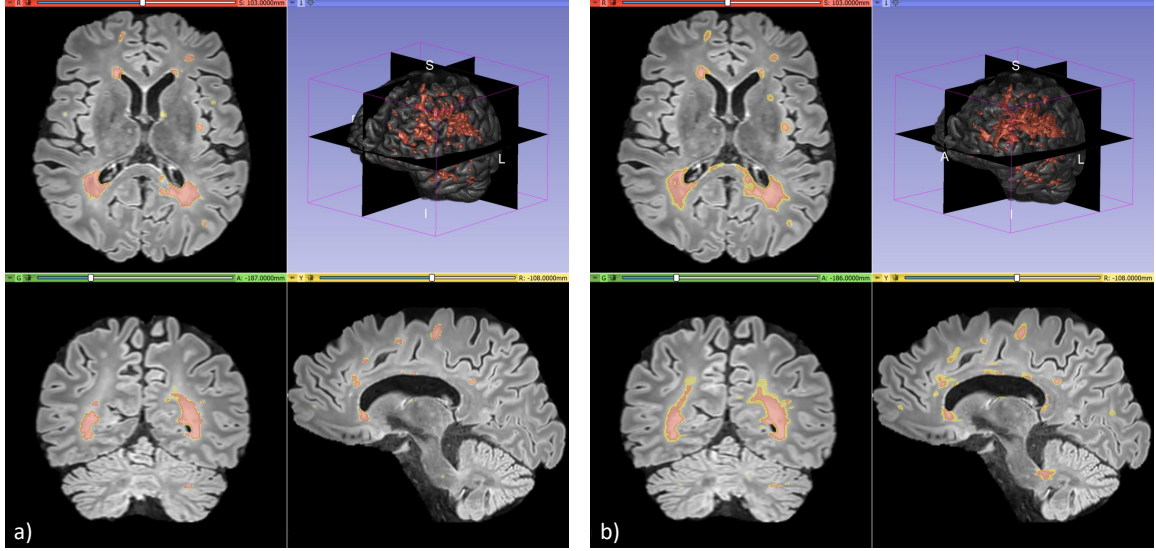
17

Draft

Figure 9: Comparison between the ternary ground truth (left) and the proposed automated framework (right). Lesion is red and Uncertainty is yellow. For readability purposes, the upper right panel of each side show just the healthy brain and Lesion in 3D.
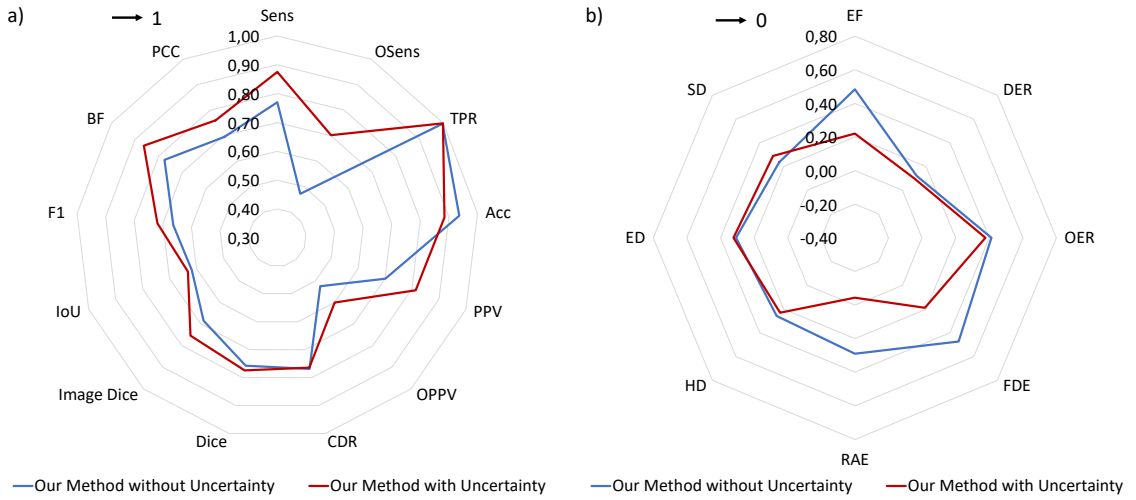

Figure 10: The proposed method when trained without and with Uncertainty, compared both on metrics whose ideal value is 1 (a) and for metrics whose ideal value is 0 (b).

of MRI and of each single modality, described above, the usage of a single modality, if sufficient, could increase the performance with respect of using multiple modality because it could contribute to stabilize the automatic strategy; b) the acquisition time and stress for the patient can be reduced.

A final remark is deserved by an important factor that determined this outstanding performance of the proposed framework: the use of the ternary ground-truth for its training. Fig. 10 shows the average performance results when the proposed framework is trained without uncertainty (on the binary consensus) as compared to those obtained when trained on the ternary consensus. Though the ensemble method trained without Uncertainty outperforms similar automated strategies (team fusion in [19]), it is far from humans: the step toward humans is evident by considering Uncertainty.

This is in line with what reported in [27, 35, 36] and it can be justified because the framework learns better what is surely Lesion, what is surely Background and uses Uncertainty for doubts, as a buffer class. Indeed, the polarized and ambiguous classification of doubtful voxels, sometimes as Lesion and others as Background, disorients an automated strategy and deviates it from the correct reasoning.

Draft

Table 2: Comparison between the proposed framework and the state of the art methods. Average data are reported for each metric and the symbol '-' is used when data are unavailable. The reported metrics are those on which at least one method different from the proposed framework has been evaluated.

Method	MRI mod.	Sens	OSens	TPR	Acc	PPV	OPPV	Dice	F1	SD
Team Fusion in [19]	FLAIR, PD, T2 T1, G-E T1	0.71	0,60	0.99	-	0.65	0.53	0.64	0.50	0.91
[26]	FLAIR, PD, T2 T1, G-E T1	0.65	-	0.86	0.97	-	-	0.76	-	-
[70]	FLAIR, T1	0.55	-	-	-	-	0.79	0.63	-	-
[4]	FLAIR, PD T1, G-E T1	0.76	-	-	-	-	-	0.82	-	-
[44]	FLAIR, T1, T2	-	-	-	-	-	-	0.76	0.59	-
Our Method	FLAIR	0.88	0.77	0.98	0.88	0.81	0.81	0.77	0.72	0.27

6 Conclusion and future work

An automated framework for the identification/segmentation of MS lesions from FLAIR MRI images has been presented. We demonstrated that traditional CNN architectures, if placed in a context that emulates the procedures of human specialists, could be effectively behave like a human expert. The strength points of the proposed framework are the following: 1) to train the system both to recognize lesions as themselves and with respect to the environment they are immersed, thus allowing to incorporate also a sort of meta-information regarding the environment where MS lesions mostly occur; 2) to resemble radiologists in consulting axial slices to discover potential lesions and to check radial and sagittal slices for confirmation and to maintain 3D continuity to their findings; 3) to use an ensemble classification that usually performs better than its components; 4) to use an artificially generated Uncertainty class to improve the performance of an automated strategy and, also for this aspect, to make it more similar to the human reasoning; 5) to operate just on FLAIR images.

Results have shown that the proposed framework resembles human raters both in behaviour and in performance, when compared with the MSSEG consensus on Lesion. Indeed, Wicoxon statistical test assessed the framework's ability to exhibit a behavior that is equivalent to, or indistinguishable from, that of a human rater.

Results also confirmed that the proposed framework outperforms the state of the art strategies which have been trained, validated and tested on the MSSEG data set. Regarding the Uncertainty class, a comparison was impossible because human segmentation of Uncertainty is unavailable. However, results have demonstrated that the usage of Uncertainty class during training greatly helps to improve the performance of the framework with respect to not using it.

In a recent report [32], the JASON Advisory Group has identified several key recommendations for advancing computation technology into routine clinical practice. One of them is that new technologies should address a significant clinical need, has to be practical in use and has to reduce medical system costs. The demonstration that a better performance is possible by including some concepts (Uncertainty and Ensemble) to enrich traditional CNN architectures, more than continuing to search for even more complex single CNN architectures, goes in the direction of the previous Jason recommendation.

Future directions of exploration will be: 1) the usage of specific pre-processing strategy for the FLAIR images, such that proposed in [51], to further improve the robustness of the method with respect to MRI and MRI scanners variability; 2) to check if the use of multiple imaging sequences could really contribute to a performance drop more than to the performance improvement; 2) the usage of a different loss function, such that proposed in [76], for better dealing with the problem of class unbalancing; 3) to study a "soft" consensus based on a single class (lesion) with different probability values, similarly to that proposed in [27], to reduce problem complexity; 4) related to the previous point #3, to explore a "soft" loss function, similar to [35], to better deal with "soft" consensus; 5) to use, besides FLAIR images, also complementary imaging modalities such as MPRAGE and MP2RAGE, to identify/segment, besides

WM lesion, also cortical lesions, similarly to [55]; 6) to test the proposed framework also for temporal MS progression (in this case, besides FLAIR, other imaging modalities, such as T_1-w, should be used to define the lesions status); 7) referred to the previous point #6, to explore specific pre-processing strategies to make all the used modalities robust with respect to MRI and MRI scanners and to avoid drops in performances when using different data set [44].

Acknowledgments

References

[1] *MSSEG Challenge Proceedings: Multiple Sclerosis Lesions Segmentation Challenge Using a Data Management and Processing Infrastructure*, Athènes, Greece, 2016. URL `https://www.hal.inserm.fr/inserm-01397806`.

[2] H. M. Rehan Afzal, Suhuai Luo, Saadallah Ramadan, and Jeannette Lechner-Scott. The emerging role of artificial intelligence in multiple sclerosis imaging. *Multiple Sclerosis Journal*, page 135245852096629, October 2020. `doi:10.1177/1352458520966298`. URL `https://doi.org/10.1177/1352458520966298`.

[3] Alireza Akhondi-Asl, Lennox Hoyte, Mark E. Lockhart, and Simon K. Warfield. A logarithmic opinion pool based STAPLE algorithm for the fusion of segmentations with associated reliability weights. *IEEE Transactions on Medical Imaging*, 33(10):1997–2009, October 2014. `doi:10.1109/tmi.2014.2329603`. URL `https://doi.org/10.1109/tmi.2014.2329603`.

[4] Ali Alijamaat, Alireza NikravanShalmani, and Peyman Bayat. Multiple sclerosis lesion segmentation from brain mri using u-net based on wavelet pooling. *International Journal of Computer Assisted Radiology and Surgery*, pages 1–9, 2021.

[5] Roohallah Alizadehsani, Mohamad Roshanzamir, Sadiq Hussain, Abbas Khosravi, Afsaneh Koohestani, Mohammad Hossein Zangooei, Moloud Abdar, Adham Beykikhoshk, Afshin Shoeibi, Assef Zare, Maryam Panahiazar, Saeid Nahavandi, Dipti Srinivasan, Amir F. Atiya, and U. Rajendra Acharya. Handling of uncertainty in medical data using machine learning and probability theory techniques: a review of 30 years (1991–2020). *Annals of Operations Research*, March 2021. `doi:10.1007/s10479-021-04006-2`. URL `https://doi.org/10.1007/s10479-021-04006-2`.

[6] Shahab Aslani, M. Dayan, L. Storelli, M. Filippi, Vittorio Murino, M. Rocca, and Diego Sona. Multi-branch convolutional neural network for multiple sclerosis lesion segmentation. *NeuroImage*, 196:1–15, 2019.

[7] L. S. Aït-Ali, S. Prima, P. Hellier, B. Carsin, G. Edan, and C. Barillot. STREM: A robust multidimensional parametric method to segment MS lesions in MRI. In *Lecture Notes in Computer Science*, pages 409–416. Springer Berlin Heidelberg, 2005. `doi:10.1007/11566465_51`. URL `https://doi.org/10.1007%2F11566465_51`.

[8] James Bergstra and Yoshua Bengio. Random search for hyper-parameter optimization. *Journal of Machine Learning Research*, 13(10):281–305, 2012. URL `http://jmlr.org/papers/v13/bergstra12a.html`.

[9] Marcel Bosc, Fabrice Heitz, Jean-Paul Armspach, Izzie Namer, Daniel Gounot, and Lucien Rumbach. Automatic change detection in multimodal serial MRI: application to multiple sclerosis lesion evolution. *NeuroImage*, 20(2):643–656, oct 2003. `doi:10.1016/s1053-8119(03)00406-3`. URL `https://doi.org/10.1016%2Fs1053-8119%2803%2900406-3`.

[10] M Brant-Zawadzki, G D Gillan, and W R Nitz. MP RAGE: a three-dimensional, t1-weighted, gradient-echo sequence–initial experience in the brain. *Radiology*, 182(3):769–775, mar 1992. `doi:10.1148/radiology.182.3.1535892`. URL `https://doi.org/10.1148%2Fradiology.182.3.1535892`.

[11] T. Brosch, L. Y. W. Tang, Y. Yoo, D. K. B. Li, A. Traboulsee, and R. Tam. Deep 3d convolutional encoder networks with shortcuts for multiscale feature integration applied to multiple sclerosis lesion segmentation. *IEEE Transactions on Medical Imaging*, 35(5):1229–1239, 2016. `doi:10.1109/TMI.2016.2528821`.

[12] Gavin Brown, Jeremy Wyatt, Rachel Harris, and Xin Yao. Diversity creation methods: a survey and categorisation. *Information Fusion*, 6(1):5–20, March 2005. `doi:10.1016/j.inffus.2004.04.004`. URL `https://doi.org/10.1016/j.inffus.2004.04.004`.

[13] Mariano Cabezas, Arnau Oliver, Sergi Valverde, Brigitte Beltran, Jordi Freixenet, Joan C. Vilanova, Lluís Ramió-Torrentà, Àlex Rovira, and Xavier Lladó. BOOST: A supervised approach for multiple sclerosis lesion segmentation. *Journal of Neuroscience Methods*, 237:108–117, nov 2014. `doi:10.1016/j.jneumeth.2014.08.024`. URL `https://doi.org/10.1016%2Fj.jneumeth.2014.08.024`.

[14] Aaron Carass, Snehashis Roy, Amod Jog, Jennifer L. Cuzzocreo, Elizabeth Magrath, Adrian Gherman, Julia Button, James Nguyen, Ferran Prados, Carole H. Sudre, Manuel Jorge Cardoso, Niamh Cawley, Olga Ciccarelli, Claudia A.M. Wheeler-Kingshott, Sébastien Ourselin, Laurence Catanese, Hrishikesh Deshpande, Pierre Maurel, Olivier Commowick, Christian Barillot, Xavier Tomas-Fernandez, Simon K. Warfield, Suthirth Vaidya, Abhijith Chunduru, Ramanathan Muthuganapathy, Ganapathy Krishnamurthi, Andrew Jesson, Tal Arbel, Oskar Maier, Heinz Handels, Leonardo O. Iheme, Devrim Unay, Saurabh Jain, Diana M. Sima, Dirk Smeets, Mohsen Ghafoorian, Bram Platel, Ariel Birenbaum, Hayit Greenspan, Pierre-Louis Bazin, Peter A. Calabresi, Ciprian M. Crainiceanu, Lotta M. Ellingsen, Daniel S. Reich, Jerry L. Prince, and Dzung L. Pham. Longitudinal multiple sclerosis lesion segmentation: Resource and challenge. *NeuroImage*, 148:77–102, mar 2017. `doi:10.1016/j.neuroimage.2016.12.064`. URL `https://doi.org/10.1016%2Fj.neuroimage.2016.12.064`.

[15] Aaron Carass, Snehashis Roy, Adrian Gherman, Jacob C. Reinhold, Andrew Jesson, Tal Arbel, Oskar Maier, Heinz Handels, Mohsen Ghafoorian, Bram Platel, Ariel Birenbaum, Hayit Greenspan, Dzung L. Pham, Ciprian M. Crainiceanu, Peter A. Calabresi, Jerry L. Prince, William R. Gray Roncal, Russell T. Shinohara, and Ipek Oguz. Evaluating white matter lesion segmentations with refined sørensen-dice analysis. *Scientific Reports*, 10(1), May 2020. `doi:10.1038/s41598-020-64803-w`. URL `https://doi.org/10.1038/s41598-020-64803-w`.

[16] Alexandre Carré, Guillaume Klausner, Myriam Edjlali, Marvin Lerousseau, Jade Briend-Diop, Roger Sun, Samy Ammari, Sylvain Reuzé, Emilie Alvarez Andres, Théo Estienne, Stéphane Niyoteka, Enzo Battistella, Maria Vakalopoulou, Frédéric Dhermain, Nikos Paragios, Eric Deutsch, Catherine Oppenheim, Johan Pallud, and Charlotte Robert. Standardization of brain MR images across machines and protocols: bridging the gap for MRI-based radiomics. *Scientific Reports*, 10(1), jul 2020. `doi:10.1038/s41598-020-69298-z`. URL `https://doi.org/10.1038%2Fs41598-020-69298-z`.

[17] Yani Chen, Bibo Shi, Zhewei Wang, Pin Zhang, Charles D. Smith, and Jundong Liu. Hippocampus segmentation through multi-view ensemble ConvNets. In *2017 IEEE 14th International Symposium on Biomedical Imaging (ISBI 2017)*. IEEE, apr 2017. `doi:10.1109/isbi.2017.7950499`. URL `https://doi.org/10.1109%2Fisbi.2017.7950499`.

[18] Dan Claudiu Ciresan, Ueli Meier, Luca Maria Gambardella, and Jurgen Schmidhuber. Convolutional neural network committees for handwritten character classification. In *2011 International Conference on Document Analysis and Recognition*. IEEE, September 2011. `doi:10.1109/icdar.2011.229`. URL `https://doi.org/10.1109/icdar.2011.229`.

[19] Olivier Commowick, Audrey Istace, Michaël Kain, Baptiste Laurent, Florent Leray, Mathieu Simon, Sorina Camarasu Pop, Pascal Girard, Roxana Améli, Jean-Christophe Ferré, Anne Kerbrat, Thomas Tourdias, Frédéric Cervenansky, Tristan Glatard, Jérémy Beaumont, Senan Doyle, Florence Forbes, Jesse Knight, April Khademi, Amirreza Mahbod, Chunliang Wang, Richard McKinley, Franca Wagner, John Muschelli, Elizabeth Sweeney, Eloy Roura, Xavier Lladó, Michel M. Santos, Wellington P. Santos, Abel G. Silva-Filho, Xavier Tomas-Fernandez, Hélène Urien, Isabelle Bloch, Sergi Valverde, Mariano Cabezas, Francisco Javier Vera-Olmos, Norberto Malpica, Charles Guttmann, Sandra Vukusic, Gilles Edan, Michel Dojat, Martin Styner, Simon K. Warfield,

François Cotton, and Christian Barillot. Objective evaluation of multiple sclerosis lesion segmentation using a data management and processing infrastructure. *Scientific Reports*, 8(1), sep 2018. `doi:10.1038/s41598-018-31911-7`. URL `https://doi.org/10.1038%2Fs41598-018-31911-7`.

[20] Gabriela Csurka, Diane Larlus, Florent Perronnin, and France Meylan. What is a good evaluation measure for semantic segmentation?. In *Bmvc*, volume 27, pages 10–5244, 2013.

[21] Antonios Danelakis, Theoharis Theoharis, and Dimitrios A. Verganelakis. Survey of automated multiple sclerosis lesion segmentation techniques on magnetic resonance imaging. *Computerized Medical Imaging and Graphics*, 70:83 – 100, 2018. ISSN 0895-6111. `doi:https://doi.org/10.1016/j.compmedimag.2018.10.002`. URL `http://www.sciencedirect.com/science/article/pii/S0895611118303227`.

[22] Massimo Filippi, Paolo Preziosa, Brenda L Banwell, Frederik Barkhof, Olga Ciccarelli, Nicola De Stefano, Jeroen J G Geurts, Friedemann Paul, Daniel S Reich, Ahmed T Toosy, Anthony Traboulsee, Mike P Wattjes, Tarek A Yousry, Achim Gass, Catherine Lubetzki, Brian G Weinshenker, and Maria A Rocca. Assessment of lesions on magnetic resonance imaging in multiple sclerosis: practical guidelines. *Brain*, 142(7):1858–1875, 06 2019. ISSN 0006-8950. `doi:10.1093/brain/awz144`. URL `https://doi.org/10.1093/brain/awz144`.

[23] Daniel García-Lorenzo, Simon Francis, Sridar Narayanan, Douglas L. Arnold, and D. Louis Collins. Review of automatic segmentation methods of multiple sclerosis white matter lesions on conventional magnetic resonance imaging. *Medical Image Analysis*, 17(1):1–18, January 2013. `doi:10.1016/j.media.2012.09.004`. URL `https://doi.org/10.1016/j.media.2012.09.004`.

[24] Ezequiel Geremia, Olivier Clatz, Bjoern H. Menze, Ender Konukoglu, Antonio Criminisi, and Nicholas Ayache. Spatial decision forests for MS lesion segmentation in multi-channel magnetic resonance images. *NeuroImage*, 57(2):378–390, July 2011. `doi:10.1016/j.neuroimage.2011.03.080`. URL `https://doi.org/10.1016/j.neuroimage.2011.03.080`.

[25] Nils Gessert, Julia Krüger, Roland Opfer, Ann-Christin Ostwaldt, Praveena Manogaran, Hagen H. Kitzler, Sven Schippling, and Alexander Schlaefer. Multiple sclerosis lesion activity segmentation with attention-guided two-path CNNs. *Computerized Medical Imaging and Graphics*, 84:101772, September 2020. `doi:10.1016/j.compmedimag.2020.101772`. URL `https://doi.org/10.1016/j.compmedimag.2020.101772`.

[26] Palash Ghosal, Pindi Krishna Chandra Prasad, and Debashis Nandi. A light weighted deep learning framework for multiple sclerosis lesion segmentation. In *2019 Fifth International Conference on Image Information Processing (ICIIP)*, pages 526–531. IEEE, 2019.

[27] Charley Gros, Andreanne Lemay, and Julien Cohen-Adad. Softseg: Advantages of soft versus binary training for image segmentation. *Medical Image Analysis*, 71:102038, 2021.

[28] Nicolas Guizard, Pierrick Coupé, Vladimir S. Fonov, Jose V. Manjón, Douglas L. Arnold, and D. Louis Collins. Rotation-invariant multi-contrast non-local means for MS lesion segmentation. *NeuroImage: Clinical*, 8:376–389, 2015. `doi:10.1016/j.nicl.2015.05.001`. URL `https://doi.org/10.1016%2Fj.nicl.2015.05.001`.

[29] R. Harmouche, L. Collins, D. Arnold, S. Francis, and T. Arbel. Bayesian ms lesion classification modeling regional and local spatial information. In *18th International Conference on Pattern Recognition (ICPR06)*. IEEE, 2006. `doi:10.1109/icpr.2006.318`. URL `https://doi.org/10.1109%2Ficpr.2006.318`.

[30] S. R. Hashemi, S. S. Mohseni Salehi, D. Erdogmus, S. P. Prabhu, S. K. Warfield, and A. Gholipour. Asymmetric loss functions and deep densely-connected networks for highly-imbalanced medical image segmentation: Application to multiple sclerosis lesion detection. *IEEE Access*, 7:1721–1735, 2019. `doi:10.1109/ACCESS.2018.2886371`.

[31] Elad Hazan, Adam Klivans, and Yang Yuan. Hyperparameter optimization: a spectral approach. In *International Conference on Learning Representations*, 2018. URL `https://openreview.net/forum?id=H1zriGeCZ`.

[32] JASON. Artificial intelligence for health and heath care. *JSR-17-Task-002*, 2017.

[33] Guixia Kang, Beibei Hou, Yiyuan Ma, Fabrice Labeau, Zichen Su, et al. Acu-net: A 3d attention context u-net for multiple sclerosis lesion segmentation. In *ICASSP 2020-2020 IEEE International Conference on Acoustics, Speech and Signal Processing (ICASSP)*, pages 1384–1388. IEEE, 2020.

[34] Z. Karimaghaloo, M. Shah, S. J. Francis, D. L. Arnold, D. L. Collins, and T. Arbel. Automatic detection of gadolinium-enhancing multiple sclerosis lesions in brain mri using conditional random fields. *IEEE Transactions on Medical Imaging*, 31(6):1181–1194, 2012. `doi:10.1109/TMI.2012.2186639`.

[35] Eytan Kats, Jacob Goldberger, and Hayit Greenspan. Soft labeling by distilling anatomical knowledge for improved MS lesion segmentation. In *2019 IEEE 16th International Symposium on Biomedical Imaging (ISBI 2019)*. IEEE, apr 2019. `doi:10.1109/isbi.2019.8759518`. URL `https://doi.org/10.1109%2Fisbi.2019.8759518`.

[36] Eytan Kats, Jacob Goldberger, and Hayit Greenspan. A soft STAPLE algorithm combined with anatomical knowledge. In *Lecture Notes in Computer Science*, pages 510–517. Springer International Publishing, 2019. `doi:10.1007/978-3-030-32248-9_57`. URL `https://doi.org/10.1007%2F978-3-030-32248-9_57`.

[37] Amrita Kaur, Lakhwinder Kaur, and Ashima Singh. State-of-the-art segmentation techniques and future directions for multiple sclerosis brain lesions. *Archives of Computational Methods in Engineering*, feb 2020. `doi:10.1007/s11831-020-09403-7`. URL `https://doi.org/10.1007%2Fs11831-020-09403-7`.

[38] Tobias Kober, Cristina Granziera, Delphine Ribes, Patrick Browaeys, Myriam Schluep, Reto Meuli, Richard Frackowiak, Rolf Gruetter, and Gunnar Krueger. MP2rage multiple sclerosis magnetic resonance imaging at 3 t. *Investigative Radiology*, 47(6):346–352, jun 2012. `doi:10.1097/rli.0b013e31824600e9`. URL `https://doi.org/10.1097%2Frli.0b013e31824600e9`.

[39] Ludmila I. Kuncheva and Christopher J. Whitaker. *Machine Learning*, 51(2):181–207, 2003. `doi:10.1023/a:1022859003006`. URL `https://doi.org/10.1023/a:1022859003006`.

[40] Alexey Kurakin, Ian J. Goodfellow, and Samy Bengio. Adversarial examples in the physical world. In *5th International Conference on Learning Representations, ICLR 2017, Toulon, France, April 24-26, 2017, Workshop Track Proceedings*. OpenReview.net, 2017. URL `https://openreview.net/forum?id=HJGU3Rodl`.

[41] Y. Lecun, L. Bottou, Y. Bengio, and P. Haffner. Gradient-based learning applied to document recognition. *Proceedings of the IEEE*, 86(11):2278–2324, 1998. `doi:10.1109/5.726791`.

[42] Geert Litjens, Thijs Kooi, Babak Ehteshami Bejnordi, Arnaud Arindra Adiyoso Setio, Francesco Ciompi, Mohsen Ghafoorian, Jeroen A.W.M. van der Laak, Bram van Ginneken, and Clara I. Sánchez. A survey on deep learning in medical image analysis. *Medical Image Analysis*, 42:60–88, dec 2017. `doi:10.1016/j.media.2017.07.005`. URL `https://doi.org/10.1016%2Fj.media.2017.07.005`.

[43] Xavier Lladó, Arnau Oliver, Mariano Cabezas, Jordi Freixenet, Joan C. Vilanova, Ana Quiles, Laia Valls, Lluís Ramió-Torrentà, and Àlex Rovira. Segmentation of multiple sclerosis lesions in brain MRI: A review of automated approaches. *Information Sciences*, 186(1):164–185, mar 2012. `doi:10.1016/j.ins.2011.10.011`. URL `https://doi.org/10.1016%2Fj.ins.2011.10.011`.

[44] Richard McKinley, Rik Wepfer, Fabian Aschwanden, Lorenz Grunder, Raphaela Muri, Christian Rummel, Rajeev Verma, Christian Weisstanner, Mauricio Reyes, Anke Salmen, et al. Simultaneous lesion and brain segmentation in multiple sclerosis using deep neural networks. *Scientific reports*, 11(1):1–11, 2021.

[45] F. Milletari, N. Navab, and S. Ahmadi. V-net: Fully convolutional neural networks for volumetric medical image segmentation. In *2016 Fourth International Conference on 3D Vision (3DV)*, pages 565–571, 2016. `doi:10.1109/3DV.2016.79`.

[46] Daryoush Mortazavi, Abbas Z. Kouzani, and Hamid Soltanian-Zadeh. Segmentation of multiple sclerosis lesions in MR images: a review. *Neuroradiology*, 54(4):299–320, may 2011. `doi:10.1007/s00234-011-0886-7`. URL `https://doi.org/10.1007%2Fs00234-011-0886-7`.

[47] Tanya Nair, Doina Precup, Douglas L. Arnold, and Tal Arbel. Exploring uncertainty measures in deep networks for multiple sclerosis lesion detection and segmentation. *Medical Image Analysis*, 59:101557, 2020. ISSN 1361-8415. `doi:https://doi.org/10.1016/j.media.2019.101557`. URL `https://www.sciencedirect.com/science/article/pii/S1361841519300994`.

[48] F Nelson, A Poonawalla, P Hou, JS Wolinsky, and PA Narayana. 3d MPRAGE improves classification of cortical lesions in multiple sclerosis. *Multiple Sclerosis Journal*, 14(9):1214–1219, oct 2008. `doi:10.1177/1352458508094644`. URL `https://doi.org/10.1177%2F1352458508094644`.

[49] Joshua Peterson, Ruairidh Battleday, Thomas Griffiths, and Olga Russakovsky. Human uncertainty makes classification more robust. In *2019 IEEE/CVF International Conference on Computer Vision (ICCV)*. IEEE, October 2019. `doi:10.1109/iccv.2019.00971`. URL `https://doi.org/10.1109/iccv.2019.00971`.

[50] G. Placidi. Mri: Essentials for innovative technologies (1st ed.). `https://doi.org/10.1201/b11868`, 2012.

[51] Giuseppe Placidi and Matteo Polsinelli. Local contrast normalization to improve preprocessing in mri of the brain. In *Proceedings of the BIOMESIP 2021*, BIOMESIP'21, page 1–12, CC, 2021. PP.

[52] Giuseppe Placidi, Luigi Cinque, Matteo Polsinelli, Alessandra Splendiani, and Emanuele Tommasino. Automatic framework for multiple sclerosis follow-up by magnetic resonance imaging for reducing contrast agents. In *International Conference on Image Analysis and Processing*, pages 367–378. Springer, 2019.

[53] Olaf Ronneberger, Philipp Fischer, and Thomas Brox. U-net: Convolutional networks for biomedical image segmentation. In *International Conference on Medical image computing and computer-assisted intervention*, pages 234–241. Springer, 2015.

[54] Francesco La Rosa, Mário João Fartaria, Tobias Kober, Jonas Richiardi, Cristina Granziera, Jean-Philippe Thiran, and Meritxell Bach Cuadra. Shallow vs deep learning architectures for white matter lesion segmentation in the early stages of multiple sclerosis. In *Brainlesion: Glioma, Multiple Sclerosis, Stroke and Traumatic Brain Injuries*, pages 142–151. Springer International Publishing, 2019. `doi:10.1007/978-3-030-11723-8_14`. URL `https://doi.org/10.1007%2F978-3-030-11723-8_14`.

[55] Francesco La Rosa, Ahmed Abdulkadir, Mário João Fartaria, Reza Rahmanzadeh, Po-Jui Lu, Riccardo Galbusera, Muhamed Barakovic, Jean-Philippe Thiran, Cristina Granziera, and Merixtell Bach Cuadra. Multiple sclerosis cortical and WM lesion segmentation at 3t MRI: a deep learning method based on FLAIR and MP2rage. *NeuroImage: Clinical*, 27:102335, 2020. `doi:10.1016/j.nicl.2020.102335`. URL `https://doi.org/10.1016/j.nicl.2020.102335`.

[56] Eloy Roura, Arnau Oliver, Mariano Cabezas, Sergi Valverde, Deborah Pareto, Joan C. Vilanova, Lluís Ramió-Torrentà, Àlex Rovira, and Xavier Lladó. A toolbox for multiple sclerosis lesion segmentation. *Neuroradiology*, 57(10):1031–1043, jul 2015. `doi:10.1007/s00234-015-1552-2`. URL `https://doi.org/10.1007%2Fs00234-015-1552-2`.

[57] Snehashis Roy, Aaron Carass, Jerry L Prince, and Dzung L Pham. Subject specific sparse dictionary learning for atlas based brain mri segmentation. In *International Workshop on Machine Learning in Medical Imaging*, pages 248–255. Springer, 2014.

[58] Snehashis Roy, John A. Butman, Daniel S. Reich, Peter A. Calabresi, and Dzung L. Pham. Multiple sclerosis lesion segmentation from brain mri via fully convolutional neural networks, 2018.

[59] Mostafa Salem, Sergi Valverde, Mariano Cabezas, Deborah Pareto, Arnau Oliver, Joaquim Salvi, Àlex Rovira, and Xavier Lladó. A fully convolutional neural network for new t2-w lesion detection in multiple sclerosis. *NeuroImage: Clinical*, 25:102149, 2020. `doi:10.1016/j.nicl.2019.102149`. URL `https://doi.org/10.1016/j.nicl.2019.102149`.

[60] Shibani Santurkar, Dimitris Tsipras, Andrew Ilyas, and Aleksander Mądry. How does batch normalization help optimization? In *Proceedings of the 32nd International Conference on Neural Information Processing Systems*, NIPS'18, page 2488–2498, Red Hook, NY, USA, 2018. Curran Associates Inc.

Draft

[61] Paul Schmidt, Christian Gaser, Milan Arsic, Dorothea Buck, Annette Förschler, Achim Berthele, Muna Hoshi, Rüdiger Ilg, Volker J. Schmid, Claus Zimmer, Bernhard Hemmer, and Mark Mühlau. An automated tool for detection of FLAIR-hyperintense white-matter lesions in multiple sclerosis. *NeuroImage*, 59(4):3774–3783, feb 2012. `doi:10.1016/j.neuroimage.2011.11.032`. URL `https://doi.org/10.1016%2Fj.neuroimage.2011.11.032`.

[62] Navid Shiee, Pierre-Louis Bazin, Arzu Ozturk, Daniel S. Reich, Peter A. Calabresi, and Dzung L. Pham. A topology-preserving approach to the segmentation of brain images with multiple sclerosis lesions. *NeuroImage*, 49(2):1524–1535, jan 2010. `doi:10.1016/j.neuroimage.2009.09.005`. URL `https://doi.org/10.1016%2Fj.neuroimage.2009.09.005`.

[63] Jasper Snoek, Hugo Larochelle, and Ryan P. Adams. Practical bayesian optimization of machine learning algorithms. In *Proceedings of the 25th International Conference on Neural Information Processing Systems - Volume 2*, NIPS'12, page 2951–2959, Red Hook, NY, USA, 2012. Curran Associates Inc.

[64] Žiga Špiclin, Franjo Pernuš, Boštjan Likar, Tim Jerman, and Domen Ravnik. Dataset variability leverages white-matter lesion segmentation performance with convolutional neural network. In Elsa D. Angelini and Bennett A. Landman, editors, *Medical Imaging 2018: Image Processing*. SPIE, mar 2018. `doi:10.1117/12.2293702`. URL `https://doi.org/10.1117%2F12.2293702`.

[65] M.D. Lawrence Steinman. Multiple sclerosis: A coordinated immunological attack against myelin in the central nervous system. *Cell*, 85(3):299–302, 2021/01/07 1996. `doi:10.1016/S0092-8674(00)81107-1`. URL `https://doi.org/10.1016/S0092-8674(00)81107-1`.

[66] M. Strumia, F. R. Schmidt, C. Anastasopoulos, C. Granziera, G. Krueger, and T. Brox. White matter ms-lesion segmentation using a geometric brain model. *IEEE Transactions on Medical Imaging*, 35(7):1636–1646, 2016. `doi:10.1109/TMI.2016.2522178`.

[67] A Traboulsee, JH Simon, L Stone, E Fisher, DE Jones, A Malhotra, SD Newsome, Jiwon Oh, DS Reich, N Richert, et al. Revised recommendations of the consortium of ms centers task force for a standardized mri protocol and clinical guidelines for the diagnosis and follow-up of multiple sclerosis. *American Journal of Neuroradiology*, 37(3):394–401, 2016.

[68] S. Vaidya, Abhijith Chunduru, Ramanathan Muthuganapathy, and G. Krishnamurthi. Longitudinal multiple sclerosis lesion segmentation using 3d convolutional neural networks. In *In Proc. International symposium on biomedical imaging, New York.*, 2015. URL `https://pdfs.semanticscholar.org/5381/da6a2ec8b7a74b85f7ffcd4ea27a2c074ddf.pdf?_ga=2.171320547.276407026.1559123876-787352723.1559123876`.

[69] Sergi Valverde, Mariano Cabezas, Eloy Roura, Sandra González-Villà, Deborah Pareto, Joan C. Vilanova, Lluís Ramió-Torrentà, Àlex Rovira, Arnau Oliver, and Xavier Lladó. Improving automated multiple sclerosis lesion segmentation with a cascaded 3d convolutional neural network approach. *NeuroImage*, 155:159–168, jul 2017. `doi:10.1016/j.neuroimage.2017.04.034`. URL `https://doi.org/10.1016%2Fj.neuroimage.2017.04.034`.

[70] Sergi Valverde, Mostafa Salem, Mariano Cabezas, Deborah Pareto, Joan C. Vilanova, Lluís Ramió-Torrentà, Àlex Rovira, Joaquim Salvi, Arnau Oliver, and Xavier Lladó. One-shot domain adaptation in multiple sclerosis lesion segmentation using convolutional neural networks. *NeuroImage: Clinical*, 21:101638, 2019. `doi:10.1016/j.nicl.2018.101638`. URL `https://doi.org/10.1016%2Fj.nicl.2018.101638`.

[71] Yeeleng S Vang, Yingxin Cao, Peter D Chang, Daniel S Chow, Alexander U Brandt, Friedemann Paul, Michael Scheel, and Xiaohui Xie. Synergynet: a fusion framework for multiple sclerosis brain mri segmentation with local refinement. In *2020 IEEE 17th International Symposium on Biomedical Imaging (ISBI)*, pages 131–135. IEEE, 2020.

[72] David S Wack, Michael G Dwyer, Niels Bergsland, Carol Di Perri, Laura Ranza, Sara Hussein, Deepa Ramasamy, Guy Poloni, and Robert Zivadinov. Improved assessment of multiple sclerosis lesion segmentation agreement via detection and outline error estimates. *BMC Medical Imaging*, 12(1), July 2012. `doi:10.1186/1471-2342-12-17`. URL `https://doi.org/10.1186/1471-2342-12-17`.

Draft

[73] S. K. Warfield, K. H. Zou, and W. M. Wells. Simultaneous truth and performance level estimation (staple): an algorithm for the validation of image segmentation. *IEEE Transactions on Medical Imaging*, 23(7):903–921, 2004. `doi:10.1109/TMI.2004.828354`.

[74] Y. Yoo, T. Brosch, A. Traboulsee, D. Li, and R. Tam. Deep learning of image features from unlabeled data for multiple sclerosis lesion segmentation. In *MLMI*, 2014.

[75] H. Zhang and Ipek Oguz. Multiple sclerosis lesion segmentation - a survey of supervised cnn-based methods. *ArXiv*, abs/2012.08317, 2020.

[76] Hang Zhang, Jinwei Zhang, Rongguang Wang, Qihao Zhang, Susan A Gauthier, Pascal Spincemaille, Thanh D Nguyen, and Yi Wang. Geometric loss for deep multiple sclerosis lesion segmentation. In *2021 IEEE 18th International Symposium on Biomedical Imaging (ISBI)*, pages 24–28. IEEE, 2021.

[77] Xiang Zhang, Xiaocong Chen, Lina Yao, Chang Ge, and Manqing Dong. Deep neural network hyperparameter optimization with orthogonal array tuning. In *International conference on neural information processing*, pages 287–295. Springer, 2019.

[78] Mariana Zurita, Cristian Montalba, Tomás Labbé, Juan Pablo Cruz, Josué Dalboni da Rocha, Cristián Tejos, Ethel Ciampi, Claudia Cárcamo, Ranganatha Sitaram, and Sergio Uribe. Characterization of relapsing-remitting multiple sclerosis patients using support vector machine classifications of functional and diffusion MRI data. *NeuroImage: Clinical*, 20:724–730, 2018. `doi:10.1016/j.nicl.2018.09.002`. URL `https://doi.org/10.1016/j.nicl.2018.09.002`.

[79] Özgün Çiçek, Ahmed Abdulkadir, Soeren S. Lienkamp, Thomas Brox, and Olaf Ronneberger. 3d u-net: Learning dense volumetric segmentation from sparse annotation. In *Medical Image Computing and Computer-Assisted Intervention – MICCAI 2016*, pages 424–432. Springer International Publishing, 2016. `doi:10.1007/978-3-319-46723-8_49`. URL `https://doi.org/10.1007%2F978-3-319-46723-8_49`.